

## Saharan Mineral Dust Experiments SAMUM-1 and SAMUM-2: what have we learned?

Albert Ansmann, Andreas Petzold, Konrad Kandler, Ina Tegen, Manfred Wendisch, Detlef Müller, Bernadett Weinzierl, Thomas Müller & Jost Heintzenberg

To cite this article: Albert Ansmann, Andreas Petzold, Konrad Kandler, Ina Tegen, Manfred Wendisch, Detlef Müller, Bernadett Weinzierl, Thomas Müller & Jost Heintzenberg (2011) Saharan Mineral Dust Experiments SAMUM-1 and SAMUM-2: what have we learned?, *Tellus B: Chemical and Physical Meteorology*, 63:4, 403-429, DOI: [10.1111/j.1600-0889.2011.00555.x](https://doi.org/10.1111/j.1600-0889.2011.00555.x)

To link to this article: <https://doi.org/10.1111/j.1600-0889.2011.00555.x>



© 2011 John Wiley & Sons A/S



Published online: 18 Jan 2017.



Submit your article to this journal [↗](#)



Article views: 19



View related articles [↗](#)



Citing articles: 2 View citing articles [↗](#)

# Saharan Mineral Dust Experiments SAMUM–1 and SAMUM–2: what have we learned?

By ALBERT ANSMANN<sup>1\*</sup>, ANDREAS PETZOLD<sup>2</sup>, KONRAD KANDLER<sup>3</sup>, INA TEGEN<sup>1</sup>, MANFRED WENDISCH<sup>4</sup>, DETLEF MÜLLER<sup>1,5</sup>, BERNADETT WEINZIERL<sup>2</sup>, THOMAS MÜLLER<sup>1</sup> and JOST HEINTZENBERG<sup>1</sup>, <sup>1</sup>Leibniz–Institut für Troposphärenforschung, Permoserstr. 15, 04318 Leipzig, Germany; <sup>2</sup>Deutsches Zentrum für Luft – und Raumfahrt, Institut für Physik der Atmosphäre, Oberpfaffenhofen, 82234 Oberpfaffenhofen, Germany; <sup>3</sup>Institut für Angewandte Geowissenschaften, Technische Universität Darmstadt, Schnittspahnstr. 9, 64287 Darmstadt, Germany; <sup>4</sup>Leipziger Institut für Meteorologie, Universität Leipzig, Stephanstr. 3, 04103 Leipzig, Germany; <sup>5</sup>Gwangju Institute of Science and Technology (GIST), Atmospheric Remote Sensing Laboratory, Department of Environmental Science and Engineering, 1 Oryong-dong, Buk–Gu, Gwangju 500-712, Republic of Korea

(Manuscript received 2 November 2010; in final form 13 May 2011)

## ABSTRACT

Two comprehensive field campaigns were conducted in 2006 and 2008 in the framework of the Saharan Mineral Dust Experiment (SAMUM) project. The relationship between chemical composition, shape morphology, size distribution and optical effects of the dust particles was investigated. The impact of Saharan dust on radiative transfer and the feedback of radiative effects upon dust emission and aerosol transport were studied. Field observations (ground-based, airborne and remote sensing) and modelling results were compared within a variety of dust closure experiments with a strong focus on vertical profiling. For the first time, multiwavelength Raman/polarization lidars and an airborne high spectral resolution lidar were involved in major dust field campaigns and provided profiles of the volume extinction coefficient of the particles at ambient conditions (for the full dust size distribution), of particle-shape-sensitive optical properties at several wavelengths, and a clear separation of dust and smoke profiles allowing for an estimation of the single-scattering albedo of the biomass-burning aerosol. SAMUM–1 took place in southern Morocco close to the Saharan desert in the summer of 2006, whereas SAMUM–2 was conducted in Cape Verde in the outflow region of desert dust and biomass-burning smoke from western Africa in the winter of 2008. This paper gives an overview of the SAMUM concept, strategy and goals, provides snapshots (highlights) of SAMUM–2 observations and modelling efforts, summarizes main findings of SAMUM–1 and SAMUM–2 and finally presents a list of remaining problems and unsolved questions.

## 1. Introduction

A considerable portion of airborne particulate matter is directly emitted from arid and barren regions of the Earth which is distributed all over the globe (Prospero et al., 2002; Tegen and Schepanski, 2009). The most prominent example of this transport is the export of desert aerosol particles from the Sahara (Goudie and Middleton, 2001). Saharan dust frequently crosses the Mediterranean towards Europe (e.g. Bergametti et al., 1989; Moulin et al., 1998; Hamonou et al., 1999; Gobbi et al., 2000; Ansmann et al., 2003; Papayannis et al., 2008; Müller

et al., 2009a), western Asia (Ganor and Mamane, 1982; Ganor et al., 2010) and the tropical North Atlantic Ocean as far as the Caribbean (e.g. Prospero and Carlson, 1972; Talbot et al., 1986; Swap et al., 1996; Liu et al., 2008b) and South America (Prospero et al., 1981; Swap et al., 1992; Formenti et al., 2001; Kaufman et al., 2005; Ansmann et al., 2009b; Ben–Ami et al., 2010). Because of the importance of Saharan dust in the climate system, the 7-yr project SAMUM<sup>1</sup> (Saharan Mineral Dust Experiment, 2004–2011) was conducted with focus on the

\*Corresponding author.

e-mail: albert@tropos.de

DOI: 10.1111/j.1600-0889.2011.00555.x

<sup>1</sup> Simoom is the English name of a small and extremely hot and dry local wind in Arabia and the Sahara. Its temperature often reaches 55 °C, and its humidity sometimes falls below 5%. Intensive ground heating under cloudless sky causes the Simoom. The Arabic word means *poison wind* and refers to the wind's tendency to cause heat stroke.

properties and transport of Saharan dust particles and their interaction with solar and terrestrial radiation.

Desert aerosol particles, consisting of a mixture of mineral matter from soil erosion together with significant contributions of sulfur, nitrogen compounds, soot from regional combustion sources and particulate matter from the biosphere and marine environments, cause complex climate impacts. Dust particles scatter and absorb solar radiation, and they scatter, absorb and emit terrestrial radiation. The magnitude of direct radiative dust forcing depends on the optical properties of dust, its vertical distribution, mixing with other aerosol, cloud cover and the spectral albedo and temperature of the underlying surface or cloud (Tegen et al., 1996; Liao and Seinfeld, 1998; Myhre and Stordal, 2001; Haywood et al., 2005; Milton et al., 2008; Bierwirth et al., 2009).

Dust also influences the Earth's climate indirectly. The presence of dust may alter cloud optical properties by changing the number and mixture of cloud condensation nuclei and especially the ice nucleus concentration (Pruppacher and Klett, 1997; DeMott et al., 2003; Field et al., 2006; Ansmann et al., 2008; Ansmann et al., 2008, 2009c; Seifert et al., 2010). The efficiency of dust particles to form liquid water drops and/or ice particles may change during transport due to mixing and coating with soluble aerosol species (Levin et al., 1996; Wurzler et al., 2000; Möhler et al., 2008; Cziczo et al., 2009). This can change both the reflectivity of clouds and the formation of rain, and possibly even the lifetime of a cloud.

Many aspects of the direct and indirect effects of dust on climate are not well understood and poorly represented in atmospheric models. Thus only a rough estimate of the magnitude of direct (anthropogenic) mineral dust radiative forcing (RF) of about  $-0.3 \text{ W m}^{-2}$  to  $0.1 \text{ W m}^{-2}$  is provided in the last report of the Intergovernmental Panel for Climate Change (Forster et al., 2007). However, dust is mainly a natural aerosol and its atmospheric mass load varies largely in time and space. The anthropogenic part of the dust load currently emitted in the atmosphere is relatively small (20% or less, Tegen et al., 2004; Yoshioka et al., 2005). In addition to its role in forcing climate, climate feedback mechanisms may lead to changes in dust production whereby changes in rainfall, soil moisture, and vegetation occur in response to global warming (Mahowald and Luo, 2003; Tegen et al., 2004; Woodward et al., 2005). Dust emissions in particular, but also atmospheric transport and removal strongly and non-linearly depend on atmospheric parameters (wind and precipitation) as well as vegetation. The impact of the daily evolution of the convective mixed layer, of hot convective plumes and dust devils (Ansmann et al., 2009a), and other dust mobilization mechanisms showing a diurnal cycle (Knippertz et al., 2007; Schepanski et al., 2009) need to be further explored. In the paleoclimate record concentrations of dust in deep sea sediment and ice sheets reveal changes in atmospheric dust concentrations up to an order of magnitude or more for different climate states (Rea, 1994; Biscaye et al., 1997; Kohfeld and Harrison, 2001;

Claquin et al., 2003). Such considerable changes in dust are also likely to occur under changing climate conditions in the future.

To understand the radiative effects of dust it is crucial to characterize its optical properties. This is also a prerequisite for constructing climate projections on global and regional scales. (i) The non-spherical shape of dust particles notoriously causes problems in the parameterization of their optical properties such as the volume scattering coefficient and the scattering phase function (Dubovik et al., 2006; Wiegner et al., 2009; Müller et al., 2010b). The size distribution of dust particles is difficult to measure but is of critical importance in the estimation of dust RF (Myhre and Stordal, 2001). A diameter range from about 10 nm to several tens of micrometres (Weinzierl et al., 2009; Petzold et al., 2009; Müller et al., 2010b) must be covered by the measurements to accurately represent the impact of dust on solar and terrestrial radiation.

(ii) Another climate-relevant factor which sensitively influences cooling and heating by dust particles concerns the wavelength-dependent scattering and absorption coefficients of pure and contaminated dust particles. For a variety of dust source regions, that is, for different particle compositions, the refractive index characteristics (real and imaginary parts of the refractive index) need to be determined (Müller et al., 2009b; Petzold et al., 2009).

(iii) Spectral surface albedo must be carefully quantified (Bierwirth et al., 2009; Tegen et al., 2010) over a variety of surfaces from the bright source regions to the dark oceanic sites. This is not only necessary to allow for more realistic estimates of the direct dust effect but also to improve satellite remote sensing (Dinter et al., 2009; Kahn et al., 2009), which delivers global maps of dust loads (retrieved from radiation information) that are required in climate modelling as input to validate dust models.

(iv) There is also a strong need for vertical profiling of dust (at ambient conditions, Esselborn et al., 2009; Tesche et al., 2009a) to better understand dust advection on regional to intercontinental scales, radiative transfer and the impact of dust on cloud formation (Ansmann et al., 2008; Ansmann et al., 2009c; Seifert et al., 2010). The CALIPSO (Cloud-Aerosol Lidar and Infrared Pathfinder Satellite Observation) mission (Winker et al., 2009) provides a multiyear data set on the three-dimensional global aerosol distribution including dust height profiles over desert areas (Liu et al., 2008a; Ben-Ami et al., 2010) and in the Saharan dust outflow regime over the tropical North Atlantic (Liu et al., 2008b).

The ultimate goal of field investigations is the development of appropriate dust parameterizations for large-scale and regional weather and climate models, which predict dust production, transport within the atmosphere and removal, and the influence on the radiative energy balance and climate. A growing number of regional dust models include the feedback of dust RF on dust mobilization and transport (Pérez et al., 2006; Heindl

et al., 2008). Field campaigns are required to validate such models (Heinold et al., 2009; Müller et al., 2009a; Johnson et al., 2011) as well as satellite remote sensing retrievals (Kahn et al., 2009; Dinter et al., 2009; Christopher et al., 2008), including the CALIPSO lidar retrievals (Wandinger et al., 2010).

All performed dust field campaigns were to some extent closure experiments (Quinn et al., 1996; Bates et al., 1998; Russel and Heintzenberg, 2000). Besides radiative closure experiments, mass and optical closure studies are most important subtasks in the development of appropriate, well-evaluated and well-tested dust parameterizations to be implemented in atmospheric transport models. After a series of successful closure studies in marine conditions with little pollution (ACE 1, Bates et al., 1998) and in heavily polluted areas of North America (TARFOX, Russell et al., 1999), southern Europe (ACE 2, Raes et al., 2000), central Europe (LACE 98, Ansmann et al., 2002), southern Asia (INDOEX, Ramanathan et al., 2001), and eastern Asia (ACE-Asia, Huebert et al., 2003), the dust field studies mentioned in the next paragraph were the first specifically devoted to desert dust (non-spherical particles). Sokolik et al. (2001) recommended to arrange intensive field investigations on desert dust as column closure experiments.

Being the largest dust source in the world, North Africa has been the focus of much research on dust by the scientific community (Reid and Maring, 2003). Based on Sun photometer observations and satellite remote sensing, monthly average mid-visible optical depths of dust on the western borders of Africa are frequently above 0.4 (Holben et al., 2001; Kaufman et al., 2005). With such consistent dust emissions and continuous dust outbreaks, North Africa and the adjacent oceanic regions are a very important natural laboratory for studying the behaviour of dust and its influence on weather and climate. Several dust-related field campaigns were conducted during the last decade. The Puerto Rico Dust Experiment (PRIDE) (Reid et al., 2003) in July 2000 and the Saharan Dust Experiment (SHADE) (Tanré et al., 2003), which took place over the tropical Atlantic between the western African coast and the Cape Verde islands in September 2000, concentrated on Saharan dust during long-range transport. The Dust and Biomass-burning Experiment (DABEX) in January–February 2006 (Haywood et al., 2008), the Dust Outflow and Deposition to the Ocean (DODO) field studies (DODO1 in the winter of 2006, DODO2 in the summer of 2006) (McConnell et al., 2008) and the NASA AMMA (NAMMA) campaign in August 2006 (Chen et al., 2010) were part of the international multiyear African Monsoon Multidisciplinary Analysis (AMMA) program (Redelsperger et al., 2006). These campaigns were conducted over western Africa and the adjacent Atlantic to investigate the properties of aerosol particles in that region and their impact on weather and climate. SAMUM-2 is complementary to these efforts that were performed in the framework of the AMMA project. In addition, the United Arab Emirates Unified Aerosol Experiment (UAE<sup>2</sup>, Reid et al. 2008) focused on dust in the southern Arabian Gulf

region in August–September 2004. Despite the success of these dust-related field investigations, deficits in our understanding of dust radiation interactions remain and motivated the SAMUM project.

SAMUM was the most comprehensive dust closure experiment of all previous dust campaigns because of the strong emphasis on vertical profiling of dust optical properties at ambient humidity conditions. Three aerosol Raman/polarization lidars and an airborne High Spectral Resolution Lidar (HSRL) were involved. State-of-the-art airborne in situ observations of the particle properties, and optical and radiative effects are the second important part of the closure activities. SAMUM-1 in southern Morocco in 2006 was the first dust closure experiment in pure dust with a minimum impact of marine, anthropogenic and biogenic aerosol sources.

SAMUM-1 results were presented in a special issue of *Tellus B* (2009). A summary of key activities and findings is given by Heintzenberg (2009). This special issue (*Tellus B*, 2011) contains the SAMUM-2 results and synergistic conclusions of both campaigns. In Section 2 of this introductory paper, the concept of the SAMUM closure experiments, the two-step strategy (two field campaigns), and the instrumental approach of SAMUM-2 is presented. Section 3 contains key observations of SAMUM-2 (winter campaign). Section 4 summarizes key findings of SAMUM-1 and SAMUM-2 and what we learned from the two campaigns. These lessons learned in mind, we formulate open questions and unsolved problems in Section 5, before concluding remarks are given in Section 6.

## 2. Concept, strategy and design

The SAMUM project followed a two-step strategy (Fig. 1). During the first phase (2004–2007) we focused on pure dust near the source region. The SAMUM-1 field campaign took place in South Morocco in May and June 2006. Freshly emitted (young) dust particles as well as aged, far-transported dust plumes with little influence of anthropogenic and marine aerosol particles were observed at Ouarzazate (30.9°N, 6.9°W, 1133 m above sea level, asl) and Tinfou (30.2°N, 5.6°W, 680 m asl), 30 km south of Zagora.

Microphysical, chemical and morphological properties and optical effects (including some that are highly dependent on particle shape) were measured in situ at the ground, as column-integrated quantities, and as profiles (lidar, aircraft). Spectral surface albedo was mapped in detail over the field sites in southern Morocco. These measurements served as input and constraints for comprehensive modelling of the scattering (coefficient and phase function) and absorption characteristics, provided valuable information for RF computations, and substantially supported space-borne passive (Multiangle Imaging Spectroradiometer, MISR) and active remote sensing activities (CALIPSO). The regional dust model system COSMO (Consortium for Small-Scale Modelling) MUSCAT (Multiscale

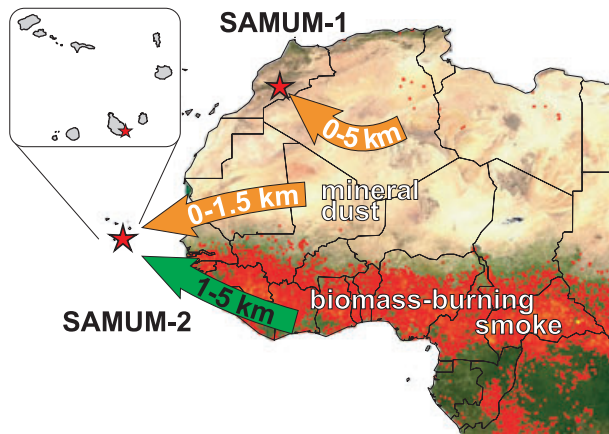


Fig. 1. SAMUM-1 and SAMUM-2 field sites (stars) in southern Morocco and at Cape Verde. Pure dust conditions prevailed during SAMUM-1 with a dust layer from the surface to about 5 km height above ground level (agl) advected from the Sahara (orange, 0–5 km). In contrast, during SAMUM-2 (winter campaign) a shallow dust layer up to about 1.5 km height agl (orange arrow, 0–1.5 km) and an extended lofted aerosol layer from about 1–5 km height agl (green arrow, 1–5 km) consisting of biomass-burning smoke and mineral dust were frequently observed. The underlying fire map derived from MODIS observations (<http://rapidfire.sci.gsfc.nasa.gov>) shows all fires (red spots) detected during the 21–30 January 2008 period.

Chemistry Aerosol Transport) was validated with the experimental data. Key results of SAMUM-1 are highlighted in section 3 of Heintzenberg (2009). Additional results of extensive closure experiments were recently published by Müller et al. (2010a,b).

SAMUM-2 focused on far-transported, aged dust and on mixtures of the dust with marine, urban and biomass-burning aerosols. Main scientific objectives were the impact of aging and mixing processes on microphysical, optical and radiative properties of Saharan dust. Two campaigns were conducted. The main field experiment took place during the winter season, a smaller one followed in the summer of 2008. SAMUM-2 was the first major field activity in the Cape Verde region to investigate both the winter (SAMUM-2a, from 15 January to 15 February 2008) and summer modes (SAMUM-2b, from 15 May to 15 June 2008) of the aerosol transport from Africa towards the Americas. More than 60 morning and afternoon/evening lidar measurement sessions were performed during the 1-month SAMUM-2a period, and about 40 morning and afternoon lidar measurement sessions within the 3.5-week SAMUM-2b intensive observation period provided a statistically significant documentation of the summer aerosol transport conditions. The earlier DODO campaigns DODO1 and DODO2 were also designed to contrast winter and summer conditions in the outflow regime west of West Africa, but only a few snapshot-like aircraft observations were realized. Lidars were not involved in the DODO study and particle size measurements could not reliably be performed for particle radii  $> 1.5 \mu\text{m}$  in that study, leading to

uncertainties in the determination of the single-scattering albedo (SSA) as discussed by McConnell et al. (2008).

During the winter campaign, a variety of very different aerosol scenarios was observed. As shown in Figs. 1 and 2 of Knippertz et al. (2011) we observed (a) shallow dust layers below optically and geometrically thick smoke/dust plumes, (b) dust layers only (up to 1.5 km height) without any smoke above, (c) smoke/dust mixtures above a clean maritime boundary layer (no dust in the lowermost 1.5 km) as well as (d) pure marine conditions without any dust and smoke throughout the troposphere. The meteorological conditions leading to such different aerosol scenarios are discussed by Knippertz et al. (2011). In contrast, the aerosol layering in summer was simple. Above the marine boundary layer (MBL) the well-known Saharan air layer was observed in the 1–6 km height range (Tesche et al., 2011a).

The SAMUM-2 field site was located north of the runway of the International Airport of Praia, the capital of the Republic of Cape Verde ( $15^\circ\text{N}$ ,  $23.5^\circ\text{W}$ , approximately 110 m asl) on island Santiago and close to the coast so that local influences (aerosol sources) on the ground-based in situ observations were minimized (prevailing wind direction is onshore from northeast). However, island effects influenced the airflow and caused disturbances in the aerosol layering in the Praia area (Engelmann et al., 2011). A sketch of the SAMUM-2 experimental activities is shown in Fig. 2. An overview of the SAMUM-2 instrumentation is given in Table 1. A detailed overview of the entire SAMUM instrumentation is given by Heintzenberg (2009) and in the individual contributions to this special issue (see references in Table 1).

Two containers were equipped with instruments for in situ observations of physico-chemical and optical properties of the boundary layer aerosol (Kandler et al., 2011a; b; Müller et al., 2011; Schladitz et al., 2011a; b). As one of the unique SAMUM activities, the spectral absorption coefficient of the desert dust particles was determined continuously during SAMUM-1 and SAMUM-2a (Müller et al., 2009b; 2011).

Three photometers (including the well-calibrated AERONET (Aerosol Robotic Network), Holben et al., 1998, travel version), four lidars and a radiosonde station were set up (Toledano et al., 2011; Tesche et al., 2011a; Groß et al., 2011a; Engelmann et al., 2011). Ground-based spectral and broad-band radiation measurements in the terrestrial and in the solar spectral ranges completed the observations at the ground station (Bauer et al., 2011; Köhler et al., 2011).

For the first time, multiwavelength Raman/polarization lidars were involved in a major dust field activity. These lidars permit us to measure height profiles of the volume extinction coefficient of the particles (directly, unambiguously, without any critical assumption) at ambient conditions, that is, at given humidity conditions and for the full dust size distribution. Furthermore the particle extinction-to-backscatter ratio and the depolarization ratio at several wavelengths are obtained. The latter parameters are highly sensitive to the shape of the light-scattering particles. By

*Fig. 2.* Schematic overview of the SAMUM-2 experiment with the METEOSAT satellite, Falcon aircraft (with downward looking lidar, green beam), ground-based lidars (green beams), radiosonde station and surface observations in and on the roof of two containers at Praia airport on Santiago island, Cape Verde. Complex layering (shown is the Falcon HSRL colour plot for the volume depolarization ratio from a flight segment on 5 February 2008, blue = marine layer, yellow-red = desert dust layer, yellow-green = smoke-dust layers) from the surface to 5 km height was observed in the majority of measurements cases.

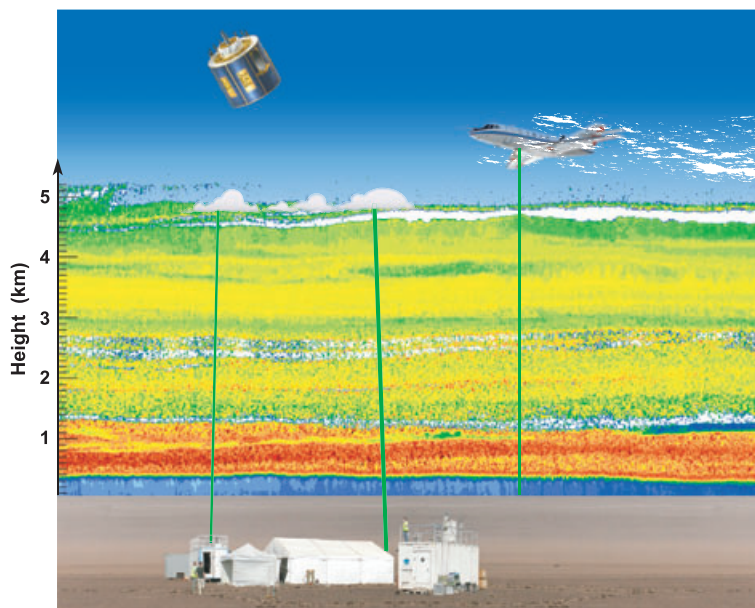


*Table 1.* SAMUM-2 instrumentation, measurement platforms, techniques applied, kind of observation and corresponding publications in which the instruments are described.

Platform/techniques	Observations	Reference
Falcon, in situ	Profiling of physical, chemical, optical and radiative properties	Weinzierl et al. (2009, 2011), Petzold et al. (2009, 2011); Kandler et al. (2009), Lieke et al. (2011), Bierwirth et al. (2009), Bauer et al. (2011)
Falcon, HSR lidar	Profiling of extinction coefficient and depolarization ratio at 532 nm, and backscatter coefficients at 532 and 1064 nm	Esselborn et al. (2008, 2009); Petzold et al. (2011), Weinzierl et al. (2011)
Praia, in situ	Physical, chemical and optical characterization at ground	Kandler et al. (2011a,b), Schladitz et al. (2011a,b), Müller et al. (2011)
Praia, Raman lidars	Profiling of extinction and backscatter coefficients and depolarization ratio at several wavelengths	Tesche et al. (2009a, 2011a); Freudenthaler et al. (2009), Groß et al. (2011a, b), Heese et al. (2009)
Praia, Doppler lidar	Profiling of horizontal and vertical wind components	Engelmann et al. (2008, 2011)
Praia, Sun photometers	Optical depth at several wavelengths	Toledano et al. (2009, 2011)
Praia, radiosonde	Temperature, pressure, humidity, horizontal wind velocity and direction	Tesche et al. (2009a, 2011a)
Praia, radiation obs.	Radiative fluxes at visible and IR wavelengths	Bauer et al. (2011), Köhler et al. (2011)

combining polarization lidar and Raman lidar techniques a clear separation of dust and smoke profiles (in terms of optical as well as microphysical properties) is possible (Tesche et al., 2009b). Raman/polarization lidars are especially useful in cases with complex layering of aerosols of different origin and vertical expansion of the aerosol layers over several kilometres. Although aerosol extinction profiling at ambient conditions (without any manipulation of the aerosol conditions before the measurement) is of fundamental importance in aerosol-related climate impact studies the employment of such state-of-the-art Raman lidars in the earlier major dust field campaigns mentioned above remained the exception (Heese and Wiegner, 2008; Johnson et al., 2008a)

rather than the rule. The ground-based SAMUM-2 aerosol lidar activities were augmented by wind Doppler lidar measurements of island effects on aerosol layering and vertical mixing (Engelmann et al., 2011).

The research aircraft Falcon 20-E of the Germany Aerospace Center (DLR) operated from Praia airport. This significantly facilitated the planning of column closure experiments. 12 flights (on 10 days) lasting 2–6 h were conducted from 19 January to 9 February. A unique feature of the Falcon observations was the potential to measure the size distribution up to 100  $\mu\text{m}$  diameter during SAMUM-1 (Weinzierl et al., 2009) and 30  $\mu\text{m}$  diameter during SAMUM-2 (Petzold et al., 2011; Weinzierl

et al., 2011). The coarse mode fraction may significantly influence the aerosol optical properties including SSA. Aboard the Falcon, an HSRL with polarization channels was operated (Esselborn et al., 2009; Weinzierl et al., 2011). Similarly to the Raman-lidar technique, the HSRL method enables profiling of the volume extinction coefficient. Together with respective radiation measurements aboard the Falcon a unique characterization of the aerosol influence on the upward radiation fluxes over the ocean and over land was possible (Bauer et al., 2011).

The SAMUM observations were augmented by a variety of models for the computation of the optical properties from the observed chemical composition, size distribution and morphology, for the calculation of the impact of extended dust fields on the radiation budget (also used in applications of satellite remote sensing), and for the simulation of regional dust and smoke transport. Details of these models are given in the SAMUM-1 special issue (Tellus 61B, 2009) and in this SAMUM-2 special issue (Gasteiger et al., 2011; Bauer et al., 2011; Köhler et al., 2011; Heinold et al., 2011a; b). SAMUM lidar and aircraft operations were synchronized to satellite overflights and the data are used for the validation of space-borne sensors and lidar backscatter profiles of the CALIPSO mission (Wandinger et al., 2010).

### 3. Key observations

As an introduction to the detailed discussions of the SAMUM-2 results in this special issue, a few measurement examples (snapshots) showing key features of the SAMUM-2 winter observations are presented. An example of dust and smoke transport

simulation is shown in addition. All SAMUM-2 topics and the list of the SAMUM-2 papers of this special issue are given in Table 2.

#### 3.1. Lidar observations of complex aerosol layering

Figure 3 shows the airborne lidar (HSRL) observation close to Praia on 5 February 2008. Remarkably complex aerosol structures were found throughout the tropospheric column up to 5 km height. Such a layering was observed on almost all days (12 flights) of the campaign. Further SAMUM-2 lidar measurement examples (height-time displays illustrating the aerosol layering) are presented by Knippertz et al. (2011), Engelmann et al. (2011), Weinzierl et al. (2011) and Tesche et al. (2011a). These aerosol conditions (dust/smoke layers above pure dust layers) as found over Cape Verde are very similar to the ones observed several hundreds to thousands of kilometres to the east during DODO1 (McConnell et al., 2008) and DABEX (Heese and Wiegner, 2008; Pelon et al., 2008; Johnson et al., 2008a).

As can be seen in Fig. 3, the MBL reached to 500–800 m height. The MBL usually contained a mixture of marine particles and desert dust (Groß et al., 2011b). Above the MBL, a shallow layer of almost pure dust extended from about 800–1500 m on that day. Soot particles (in the small particle fraction) were found in the lofted dust layer. From 1200 m to 5 km height well-stratified layers of less and strongly polluted air were observed. Shallow cumulus fields developed as well as convective plumes close to the island (there is another island about 40 km northeast of Praia). Cumulus convection and island effects

Table 2. List of SAMUM-2 research areas and special-issue papers.

Chemical composition	Kandler et al. (2011a, b), Lieke et al. (2011)
Shape properties, aspect ratio	Kandler et al. (2011a,b)
Size distribution	Weinzierl et al. (2011), Kandler et al. (2011a), Schladitz et al. (2011a)
Hygroscopic growth	Schladitz et al. (2011a)
Scattering coefficient	Müller et al. (2011), Schladitz et al. (2011b)
Absorption coefficient	Müller et al. (2011), Petzold et al. (2011), Schladitz et al. (2011b), Weinzierl et al. (2011)
Refractive index	Kandler et al. (2011b), Müller et al. (2011), Schladitz et al. (2011b), Petzold et al. (2011), Weinzierl et al. (2011)
Single-scattering albedo	Müller et al. (2011), Petzold et al. (2011), Tesche et al. (2011b)
Optical closure	Schladitz et al. (2011b), Weinzierl et al. (2011)
Optical depth spectra	Toledano et al. (2011)
Extinction coefficient profiling	Tesche et al. (2011a), Groß et al. (2011b), Petzold et al. (2011), Weinzierl et al. (2011)
Depolarization ratio (DR) profiling	Groß et al. (2011a), Weinzierl et al. (2011)
Lidar ratio (LR) profiling	Tesche et al. (2011a), Groß et al. (2011b)
DR and LR modelling	Gasteiger et al. (2011)
Inversion retrievals (microphys. prop.)	Tesche et al. (2011b), Toledano et al. (2011)
Radiative transfer, forcing	Bauer et al. (2011), Köhler et al. (2011), Torge et al. (2011)
Regional aerosol transport	Heinold et al. (2011a, b)
Dust mobilization	Knippertz et al. (2011), Heinold et al. (2011a)
Heat-island effects, vertical mixing	Engelmann et al. (2011), Weinzierl et al. (2011)
Dust mixing with urban haze	Petzold et al. (2011)

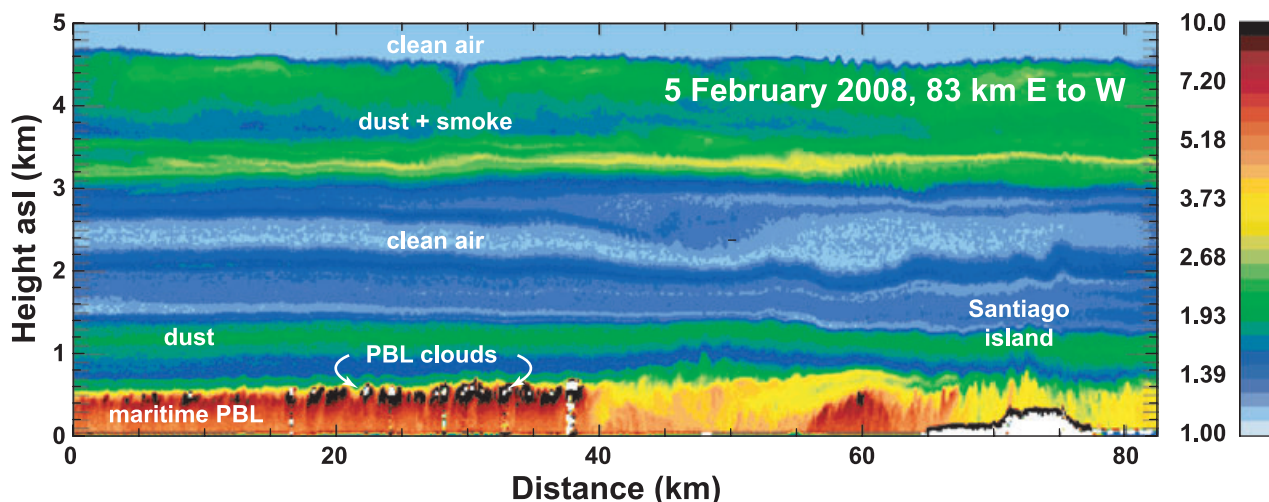


Fig. 3. 532-nm backscatter ratio (red = strong backscattering, blue = weak backscattering) measured with the airborne HSRL on 5 February 2008. The east–west flight was performed at 15°N. Santiago island extends from 65–80 km (distance scale), Praia is located at distance = 66 km. Complex, stratified aerosol layering is observed in the free troposphere. Boundary layer clouds develop between 0–40 km (distance scale). Convective motions (plumes of high backscatter) in the lowermost troposphere around the island (60–85 km) are probably caused by surface heating and roughness effects. Another island is located northeast (upwind) of Praia (around distance = 60 km).

(surface heating, surface roughness changes) triggered downward mixing of smoke and dust towards the surface. The influence of vertical mixing on the aerosol characteristics over Praia and heat island effects, that disturb the horizontal transport of aerosols, are discussed by Engelmann et al. (2011) based on Doppler lidar observations of vertical-velocity fields.

Knippertz et al. (2011) provide an extended overview of the meteorological conditions for SAMUM-2. Therefore, only a brief meteorological description is given here. As pointed out by Knippertz et al. (2011) a general feature of the synoptic situation during the SAMUM-2 winter experiment was the development of several distinct high-pressure systems in the Azores region which moved from the subtropical North Atlantic across the Iberian Peninsula into western Europe and the western Mediterranean Sea. These high-pressure systems influenced the weather in northern Africa and caused large south–north pressure gradients across the entire Sahel (see fig. 8 of Knippertz et al. 2011). Widespread dust emissions over the entire region from the Bodélé Depression to the coast of Mauritania developed. Trajectory analysis reveals that the surface–near coherent dust flow (mainly from easterly and northeasterly directions) occurs up to 1–2 km height. Such a flow pattern and vertical extension of the dust layer is in agreement with AMMA/DABEX lidar observations (Cuesta et al., 2008) and space-borne CALIPSO lidar measurements (Liu et al., 2008a) in the winter half year over the Saharan desert. Pronounced dust layers were observed above Praia at heights <1.5 km (asl) on all days during January 2008 (see fig. 1 in Knippertz et al., 2011). The high-pressure influence weakened during February 2008. The air flow in the lowermost 1–1.5 km of the troposphere frequently turned to

northerly directions so that dusty air was no longer observable in such situations.

The backward trajectory analysis and results of SAMUM-2 atmospheric transport modelling shows that Saharan dust is also advected southwards by the Harmattan winds and then mixed upwards by convection (Knippertz et al., 2011). South of about 11°N, where biomass–burning activity is most intensive (see Fig. 1), smoke is injected into the dust layer and equally mixed to greater heights. The analysis of Knippertz et al. (2011) is in agreement with the conceptual picture of aerosol layering and air flow as shown for a typical DABEX scenario in fig. 12 of Haywood et al. (2008). DABEX lidar observations in southern West Africa show mixed dust/smoke layers up to 5 km height (Pelon et al., 2008; Heese and Wiegner, 2008; Ben-Ami et al., 2010). The southerly position of the intertropical convergence zone (illustrated in fig. 5 of Tesche et al., 2011a) forces the dust/smoke plumes to travel westwards towards the tropical Atlantic. In summary, the surface–near flow of dust from easterly to northeasterly directions controlled the aerosol conditions over Cape Verde up to about 1.5 km height during extended periods of the SAMUM-2 campaign, whereas the air masses containing dust and smoke and advected from east to southeast prevailed in the height range from 1.5 to 5 km height. By assuming mean advection velocities of 10 m s<sup>-1</sup>, the aerosol particles need 1.5–4 d to travel distances of 1500–3000 km (typical distances between Cape Verde and the fire areas).

Complementary to the airborne lidar observations, the three ground-based aerosol Raman lidars almost continuously observed the aerosol layers during the 4-week period and provide extended vertically resolved statistics of particle optical properties. The full observational potential of the Raman/polarization

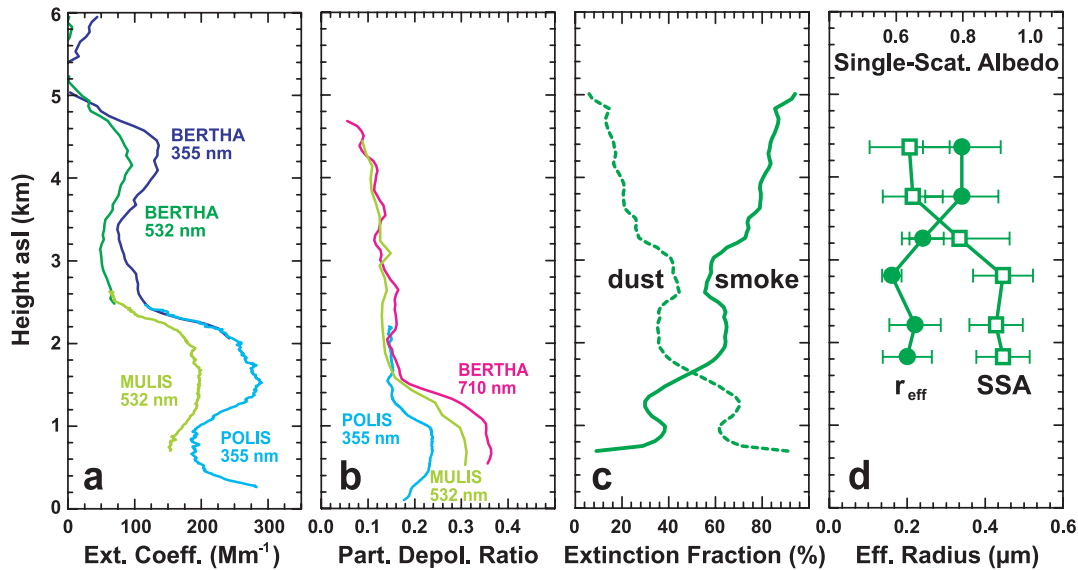


Fig. 4. (a) Raman lidar measurement of the volume extinction coefficient of particles at Praia, Cape Verde, from the dust-laden marine boundary layer to the top of the dust-smoke layer at 5 km height on 31 January 2008, (b) particle depolarization ratio, (c) dust and smoke contributions to the total volume extinction coefficients of particles and (d) retrieved smoke-related effective radius and single-scattering albedo. The measurements of three lidars (POLIS, MULIS and BERTHA) are combined. Light scattering and depolarization by mineral dust dominates up to 1.3 km. A homogeneous layer of aged smoke (a low smoke depolarization ratio  $<0.05$  is assumed) and dust is present above about 1.3 km height. 1-h average profiles are shown, lidar return signals are smoothed with window lengths of 80–600 m, statistical uncertainties in the extinction coefficients are on the order of 10%.

lidar consortium is shown in Fig. 4. A two-layer structure (see depolarization profile in Fig. 4b) was observed on 31 January 2008 with a lower layer, in which the optical properties were dominated by dust, and a lofted layer above 1500 m, in which both desert dust and biomass-burning smoke contributed to the optical effects. Volume extinction values of 150–200  $\text{Mm}^{-1}$  and 100–300  $\text{Mm}^{-1}$  are determined in the dust layer and the smoke-dominated aerosol layers, respectively. Backward trajectories for this day are shown by Tesche et al. (2009b).

As can be seen in Fig. 4b, the dust depolarization ratio is wavelength-dependent with values around 0.3 at 532 nm. The depolarization ratio of smoke is assumed to be low ( $<0.05$ , Tesche et al., 2009b) so that the linear depolarization ratio for the mixture of dust and smoke is about 0.15. By the use of the depolarization ratio information the optical properties of dust and smoke can be separated (Tesche et al., 2009b). As a result, the smoke contribution to the total particle extinction coefficient ranges from 60 to 80% in the lofted layer (Fig. 4c). The inversion of the smoke-related spectral backscatter and extinction lidar data yield microphysical properties such as the surface-area-weighted or effective radius of the smoke particles (mostly from 0.2 to 0.3  $\mu\text{m}$  in Fig. 4d) and the SSA (0.65–0.9 for 532 nm) of the highly absorbing soot (or black carbon, Andreae and Gelencsér, 2006). The 31 January 2008 case has been fully evaluated by Tesche et al. (2009b). The SSA range of 0.65–0.9 (mean value of 0.75) for pure smoke is characteristic for the entire SAMUM-2a campaign (Tesche et al., 2011b). It is interesting to note that SSA

values derived from airborne in situ observations during DABEX and SAMUM-2 indicate slightly higher SSA values (on average  $0.77\text{--}0.81 \pm 0.05$ , 530–550 nm) in smoke-dominated aerosol layers (Tesche et al., 2011b). This is probably caused by the fact that the lidar technique allows us to clearly separate the dust from the smoke, whereas the aircraft observations provide SSA values for the total fine mode including dust particles which have SSA values of  $>0.95$ . The SAMUM-2 Sun photometer observations revealed values of about 0.84 for SSA (550 nm) when the optical depth was dominated by smoke (fine mode optical depth  $>0.5$ , Toledano et al., 2011) but dust particles were present as well.

Tesche et al. (2011a,b), Groß et al. (2011a,b) and Weinzierl et al. (2011) discuss the SAMUM-2a lidar observations. Tesche et al. (2011a) also present the SAMUM-2b (summer campaign) results. Sun photometer measurements of spectral optical depth and Ångström exponent, inversion products from almucantar radiances such as particle size distribution, effective radius, fine mode fraction and particle absorption properties (including SSA values for dust or smoke-dominated aerosol columns or mixtures), and comparison with in situ observations (microphysics, SSA) complement the winter-campaign lidar studies (Toledano et al., 2011). The lidar-derived optical properties (lidar ratios and depolarization ratios) are used to improve parameterizations of dust scattering and absorption in models (Gasteiger et al., 2011). Lidar-derived extinction coefficient profiles are considered in optical closure experiments (Weinzierl et al., 2011) and in

studies of the interaction of dust particles with terrestrial radiation (Köhler et al., 2011). The Falcon lidar data (extinction coefficient profiles) are used to study the aerosol impact on upward solar radiation (Bauer et al., 2011). Heinold et al. (2011a,b) compare transport simulations with lidar observations of dust and smoke profiles for 25, 28 and 31 January 2008. In Section 3.5, we show the lidar–model comparison for 4 February 2008.

This aerosol layering of a surface–near dust layer and a mixed plume of dust and biomass-burning smoke as shown in Figs. 3 and 4 has earlier been observed over the African continent (in the biomass-burning area), about 2500–3000 km east of Cape Verde during DABEX in the winter of 2006 (Haywood et al., 2008). Complex aerosol profiles of fresh and aged fire smoke mixed with mineral dust were measured with lidars (Johnson et al., 2008a; Pelon et al., 2008; Heese and Wiegner, 2008) and during 13 flights with the research aircraft BAe146 of the UK Meteorological Office (Johnson et al., 2008a; b; Osborne et al., 2008). Top heights of the aerosol plumes typically ranged from 4 to 5 km height. This is also found by the CALIPSO lidar (Ben-Ami et al., 2010).

### 3.2. Chemical analysis

During the winter campaign, aerosol particles of mineral dust, marine and biomass-burning aerosols were collected at Praia and aboard the Falcon aircraft in a particle diameter range of approximately  $D = 0.1$  to  $20 \mu\text{m}$  (Kandler et al., 2011a; b; Lieke et al., 2011). To sample this large size range, at Praia a set of cascade impactors mounted isoaxially on a three-dimensional wind vane was used for particles smaller than  $10 \mu\text{m}$  diameter (Kandler et al., 2007). For larger particles, a free-wing impactor was deployed (Jaenicke and Junge, 1967; Kandler et al., 2009). A similar set of cascade impactors was employed aboard the Falcon aircraft for particles smaller than  $3 \mu\text{m}$  diameter, whereas larger particles were collected with a newly created Giant Particle Collector (described by Lieke et al., 2011), which consists of an

automatically interchangeable free–stream impactor mounted in an under-wing pod.

By means of electron-microscopical single particle analysis, the chemical composition, shape and state of mixing of more than 200 000 particles were investigated. Different flight patterns (Weinzierl et al., 2011) allowed for the investigation of particle aging effects as well as vertical profiling over the ground station to study aerosol layering and vertical mixing effects. The single particle analysis provided highly valuable information to complement the information deduced from remotely sensed data.

Figure 5 shows the vertical and size-resolved chemical composition of the aerosol measured over the Praia ground station on 25 January, 2008. A height–time display of aerosol layering on 25 January 2008 (airborne lidar observations) is shown by Engelmann et al. (2011). The particles were classified into different groups according to their chemical composition and morphology (for details see Kandler et al., 2011b). A very strong change of the chemical composition and particle size with height is obvious. The MBL reached up to about 650 m according to the aerosol Raman and wind Doppler lidar measurements (Groß et al., 2011a; Engelmann et al., 2011). For particles with  $D < 500 \text{ nm}$  mineral dust is the major component below 700 m height.

Soot—that is, carbonaceous particles identified explicitly by their morphology, chemical composition and internal concentric shell structure in the electron microscope (for examples see Li et al., 2003; Lieke et al., 2011)—becomes dominant at higher altitudes for the small particles, while only a minute amount of sulfate is present on this day. Despite this dominance, soot contributes only with 1% (or even less) to the total particle volume. For particles larger than 500 nm this pronounced layer structure becomes less obvious. For this size range, mineral dust is always the most abundant component. The mineral dust itself is always dominated by silicate particles, in which feldspars as well as clay minerals are present (Kandler et al., 2011a; b; Lieke et al., 2011). Iron oxides contribute in variable amounts, although no obvious influence of the atmospheric layering on their

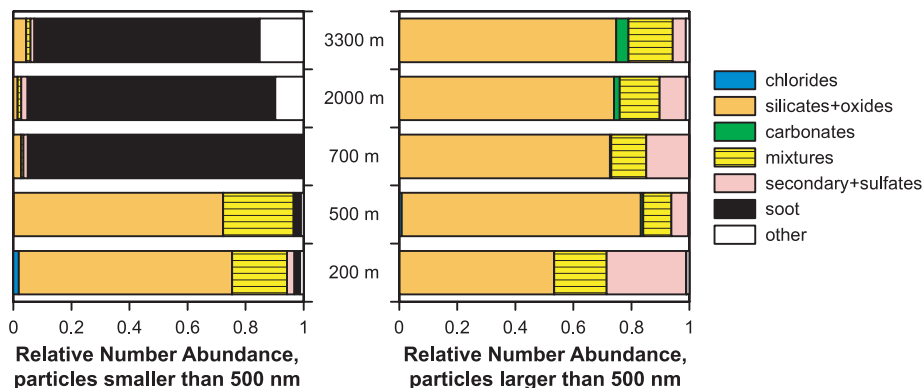


Fig. 5. Chemical composition of particles with  $D < 500 \text{ nm}$  (left-hand side) and  $D > 500 \text{ nm}$  (right-hand side) for five different height levels (asl). The measurement was performed aboard the Falcon aircraft close to Praia on 25 January 2008.

occurrence is recognizable in this case. For the larger particles with  $D > 2.5 \mu\text{m}$ , Ca-dominated particles—especially in the highest layer at 3300 m asl—were found, indicating a difference in source regions of mineral dust within the higher atmospheric layers. In contrast to the samples collected during SAMUM-1 in Morocco in 2006 (Kandler et al., 2009; Scheuven et al., 2011), quartz only has a low contribution to the dust particles. Finally, the analysis shows that sulphates contribute significantly to the aerosol in the size range from  $D = 0.5\text{--}2.5 \mu\text{m}$  (Kandler et al., 2011b; Schladitz et al., 2011a). In general, from a chemical point of view the atmospheric layering (changing aerosol composition with height) at Cape Verde during SAMUM-2 (winter campaign) was much more pronounced than over Morocco during SAMUM-1 (Kandler et al., 2009). Over Cape Verde on nearly all days a clearly visible layer structure was found (Lieke et al., 2011), while this could be detected for singular events only over Morocco. 10–20% of the silicate dust particles were internally mixed with sulphate. This relative abundance of mixtures is not significantly higher than what was found in other places closer to dust source areas (Kandler et al., 2007; 2009). Also, no significant sensitivity of the abundance of internally mixed particles to particular atmospheric layers was detected. Thus, no evidence can be provided that the mineral dust in this case was modified significantly during its transport from the source regions in western Africa (Knippertz et al., 2011) to Cape Verde, even though the dust at heights  $< 1 \text{ km}$  was directly advected from desert regions and the dust at heights  $> 1 \text{ km}$

crossed the biomass-burning areas thereby mixing with smoke aerosol.

### 3.3. *In situ characterization of optical and microphysical aerosol properties*

Parallel to the chemical characterization, optical and microphysical aerosol properties were measured at Praia (Kandler et al., 2011a; Schladitz et al., 2011a; b; Müller et al., 2011) and aboard the Falcon (Petzold et al., 2011; Weinzierl et al., 2011). Figure 6 shows the Falcon profiles of particle number concentrations, volume absorption coefficients at three wavelengths and the absorption-related Ångström exponent (Petzold et al., 2009; 2011) for the same observation as shown in Fig. 5.

A dedicated column closure study was conducted over Praia airport on 25 January 2008. The entire flight pattern was organized around the ground-based lidar and Sun photometer instruments (see height–time display of aerosol layering for this day in Engelmann et al., 2011, and Weinzierl et al., 2011). Flights across Santiago island were also performed to investigate the island effects on the air flow and aerosol layering (Engelmann et al., 2011). The tropospheric column was probed by the airborne HSRL from an altitude of approximately 10 km asl, while in situ measurements were taken during a stacked descent with constant level holding patterns at altitudes of 578, 772, 2052 and 3513 m asl.

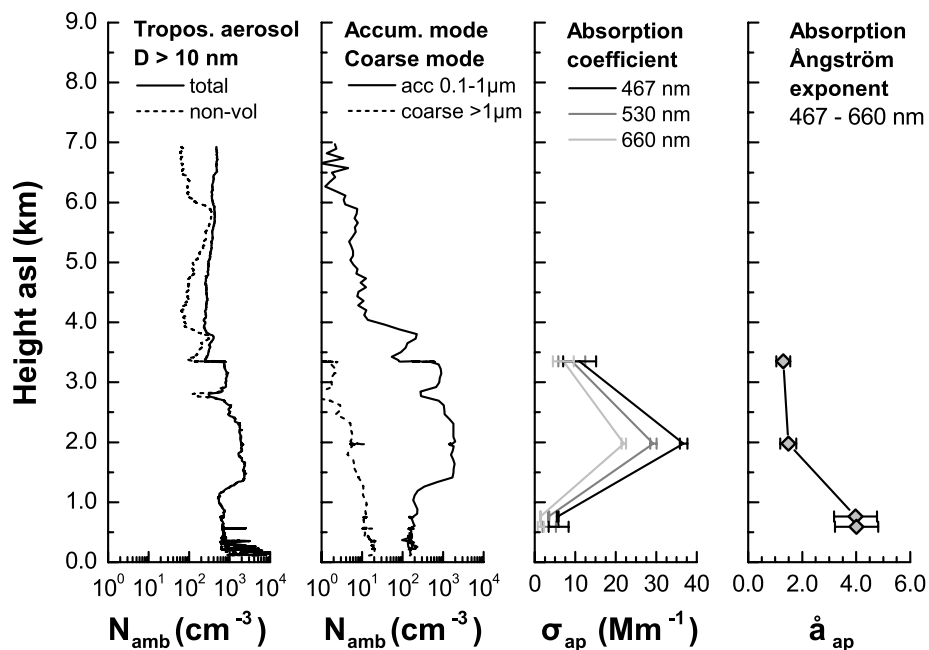


Fig. 6. Vertical profiles of in situ measured aerosol properties in the tropospheric column above Praia on 25 January 2008 (from left to right): number concentrations  $N_{\text{amb}}$  of total and non-volatile particles in the size range  $D > 10 \text{ nm}$ , number concentrations of accumulation ( $0.1 \mu\text{m} < D < 1 \mu\text{m}$ ) and coarse mode particles ( $D > 1 \mu\text{m}$ ), aerosol absorption coefficient  $\sigma_{\text{ap}}$ , and absorption-related Ångström exponent  $\dot{a}_{\text{ap}}$  computed from the wavelength pair of 467 nm and 660 nm.

On 25 January 2008, the microphysical observations indicated that dust dominated from the surface up to 1300 m. Dust particles with  $D > 3 \mu\text{m}$  (not shown in Fig. 6) were found exclusively below 1300 m. Above this height biomass-burning particles from western Africa occurred in high concentrations. Below 3.3 km height asl the number concentrations of the total and non-volatile particles were almost identical indicating that the aerosols consisted of non-volatile particles (soot and dust). Light absorption was much stronger in the biomass-burning layer ( $10\text{--}40 \text{ Mm}^{-1}$ ) than in the mineral dust layer ( $3 \text{ Mm}^{-1}$ ). However, the biomass-burning layer contributed only 42% to the particle optical thickness (AOT) derived from the HSRL extinction profile, while the dust layer contributed 54%. Peak number concentrations of  $10^4 \text{ cm}^{-3}$  in dense, fresh smoke plumes were observed during DABEX (Capes et al., 2008; Johnson et al., 2008a). In aged smoke layers, number concentrations on the order of  $10^3 \text{ cm}^{-3}$  are reported. These latter values are similar to the ones in Fig. 6 (left-hand panel).

The absorption-related Ångström exponents (wavelength range 467–660 nm) showed values of 1.2–1.4 in the smoke and values around 4 in the dust layer. For comparison, the absorption-related Ångström exponents ranged from 2.6 to 6.5 for fresh dust observed during SAMUM-1. Values for mineral dust mixed with carbonaceous particles from urban pollution (near Casablanca) were  $< 2$  during SAMUM-1. The high Ångström values that we also found for all investigated pure dust cases during SAMUM-2 (winter campaign) indicate that even after long-range transport no significant mixing with urban pollution or smoke occurred. These Ångström exponents for mineral dust observed during SAMUM-1 and SAMUM-2 are similar to the values of 4.2–5.3 determined in the laboratory for various dust samples (Linke et al., 2006). The SSA values for 530 nm were 0.78–0.8 in the smoke layer (at 2 and 3.5 km height) on 25 January 2008.

Mineral dust was also sampled in the vicinity of Dakar, Senegal (Petzold et al., 2011). In cases of dust mixed with urban pollution, absorption-related Ångström exponents of 2.7 were observed. This value is similar to samples taken near the city of Casablanca during SAMUM-1. In contrast, dust without urban pollution was characterized by absorption Ångström exponents of 4.4–5.4. Details of the effects of mixing of combustion aerosol particles with mineral dust particles are discussed by Petzold et al. (2011), in conjunction with a chemical analysis of mineral dust samples collected in the different dust layers (Lieke et al., 2011).

The Ångström exponent of 1 in Fig. 6 above 1500 m describes an absorbing aerosol composed of small particles (Petzold et al., 2009). The absorption wavelength dependence can be explained by a black carbon mass content of 8% in the biomass-burning layer, with no iron oxides present. In contrast, the mineral dust layers below 1500 m height were characterized by a black carbon mass fraction  $< 1\%$ . DABEX black carbon contents of 10–16% in the smoke/dust layers are reported (Capes et al., 2008; Johnson et al., 2008a). These values are considerably higher than the

SAMUM-2 mass fractions. However, SAMUM-2 flights were performed in aged air masses over the Atlantic whereas DABEX was focusing on the source regions of smoke. On the other hand, similar techniques used for the determination of the black carbon fraction of total aerosol mass yield black carbon mass fractions of 3–8% in aged smoke from Canadian forest fires after 6–9 d of long-range transport (Petzold et al., 2007).

Figure 7 shows particle size distributions measured on 25 January 2008 at four height levels. During SAMUM-1 close to the dust source region, particle size distributions covered the entire size range from approximately  $D = 4 \text{ nm}$  to  $100 \mu\text{m}$ . During SAMUM-2, only instruments for measuring particle size up to  $30\text{--}40 \mu\text{m}$  were installed. Instrumentation required to cover the size range up to  $100 \mu\text{m}$  was available, but not used during SAMUM-2. A detailed description of the size distribution measurements including a validation of these measurements performed during SAMUM is given in Weinzierl et al. (2009, 2011). Figure 7 (bottom panels) shows that the dust particle size distribution on 25 January 2008 is almost entirely within the envelope of the SAMUM-1 measurements. For particles with  $D < 1 \mu\text{m}$ , the dust aerosol size distributions measured during SAMUM-2 compare well with observations made during SAMUM-1. Differences are found for the size range of  $D > 10 \mu\text{m}$ . During SAMUM-1, in all cases particles with  $D > 10 \mu\text{m}$  were present, and in most cases (80%) the particles were  $< 40 \mu\text{m}$  (Weinzierl et al., 2011). In contrast, no particles with diameters close to  $30 \mu\text{m}$  were found during SAMUM-2 and in several cases even no particles with  $D > 10 \mu\text{m}$  were detected. The reason for the depletion of large coarse mode dust particles is gravitational settling during long-range transport.

The size distributions of the tropical biomass-burning aerosol from savannah fires (see top panels in Fig. 7) show some agreement with size distributions of aged Canadian boreal forest fire plumes measured over Europe after 6–9 d of long-range transport (Petzold et al., 2007). In both cases the biomass-burning aerosol mode peaks between 200 and  $300 \text{ nm}$  in diameter. Although a coarse mode with particles with  $D > 1 \mu\text{m}$  is present in both cases, the tropical biomass-burning aerosol layers measured during SAMUM-2 show a significant amount of  $10\text{--}\mu\text{m}$  particles which is not present in the boreal biomass-burning layers. This difference is explained by the fact that the tropical biomass-burning layers contained a significant amount of mineral dust particles originating from the region north of  $11^\circ\text{N}$  (Knippertz et al., 2011). Similar characteristics as shown in Fig. 7 (top panels) for aged smoke were observed during DABEX (Capes et al., 2008; Johnson et al., 2008b). More details about the presence and the origins of the large mineral dust particles observed in the lofted biomass-burning layers is given in Weinzierl et al. (2011).

Strong efforts to characterize the microphysical and optical properties of pure dust and dust mixed with marine and pollution particles were also undertaken at ground. In-depth optical closure studies, based on the surface observations at Praia,

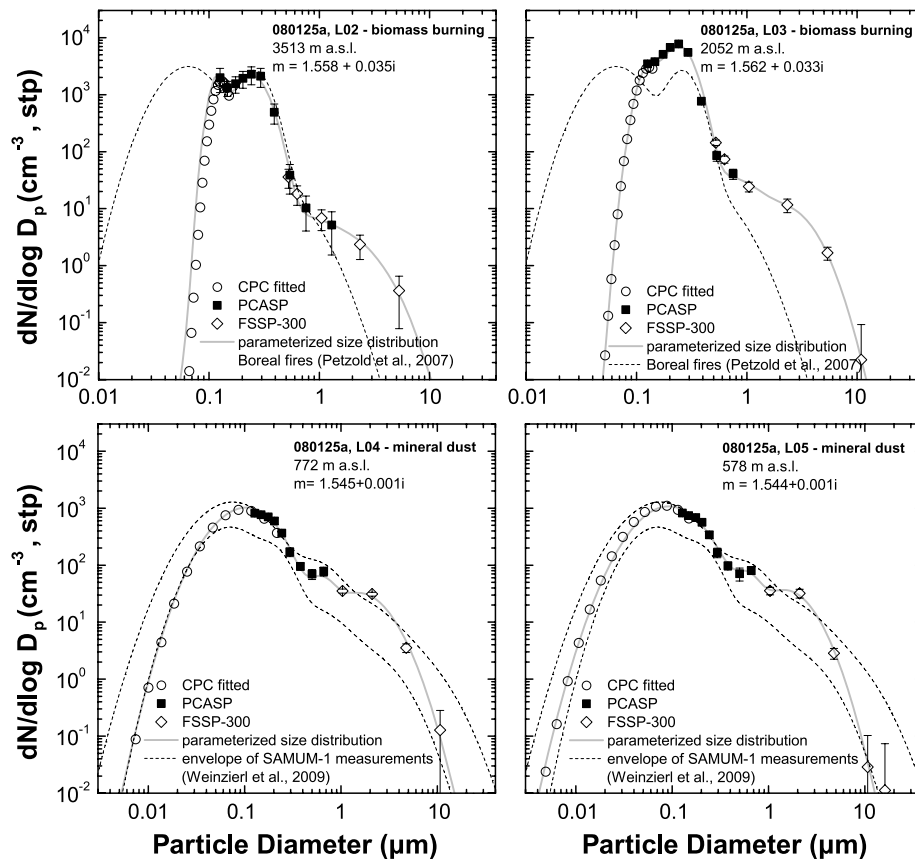


Fig. 7. Particle size distributions observed at four different altitudes in the column above Praia on 25 January 2008. The top row shows size distributions of tropical biomass-burning aerosol measured at 3513 m and 2052 m height. These constant altitude sequences correspond to layers L02 and L03 in Weinzierl et al. (2011). The bottom row shows mineral dust size distributions measured at 772 m (L04) and 578 m height (L05). Observations are given as symbols, the parameterized size distributions are presented as solid lines. For comparison, the envelope of the SAMUM-1 measurements is added. For more details regarding the observations (with CPC, PCASP and FSSP-300) and assumed refractive index in the data analysis see Weinzierl et al. (2011).

regarding scattering, absorption and extinction coefficients of particles including the dependence of the optical properties on relative humidity are presented by Schladitz et al. (2011a,b). Hygroscopic growth studies are important to connect in situ observations of optical properties (of dry particles) with respective ones from remote sensing (Groß et al., 2011b). Mineral dust particles during SAMUM-1 and during SAMUM-2 showed a nearly non-hygroscopic behaviour (Kaaften et al., 2009; Schladitz et al., 2011a).

Figure 8 presents an overview of the SAMUM-1 and SAMUM-2 surface observations of the spectral absorption coefficient and the respective imaginary part of the refractive index. The knowledge of the spectral dependence of absorption by desert dust particles and the respective complex refractive index is a fundamental pre-requisite for the modelling of the direct dust radiative effect. Absorption by dust depends on the size and shape of the particles and their mineralogical composition. As pointed out by Sokolik and Toon (1999), the imaginary part of the refractive index is strongly variable in the spectral range

from the ultraviolet to the near-infrared. The measurement of the spectral refractive index in one of the main source regions of desert dust and in the long-range transport regime is one of the highlights of the SAMUM project. Spectral absorption coefficients were measured with an absorption photometer from 300 to 800 nm during SAMUM-1 and from 300 to 960 nm during SAMUM-2. The measurement technique and data analysis procedures are outlined in Müller et al. (2009b, 2011) and Schladitz et al. (2011a; b). Since these surface measurements are done downstream of a PM10 (particulate matter,  $D < 10 \mu\text{m}$ ) inlet, all derived particle properties of in situ measurements refer to particles with aerodynamic diameters  $D_a < 10 \mu\text{m}$ . In Fig. 8, the absorption and the imaginary part of the refractive index show a strong dependence on wavelength. The spectral dependence is most pronounced when dust concentrations are high (absorption-related Ångström exponents in the wavelength range 450–650 nm are 3.9 during SAMUM-2 and 5.2 during SAMUM-1, see Fig. 8) compared to the background with a concurrent, non-negligible amount of soot (absorption-related

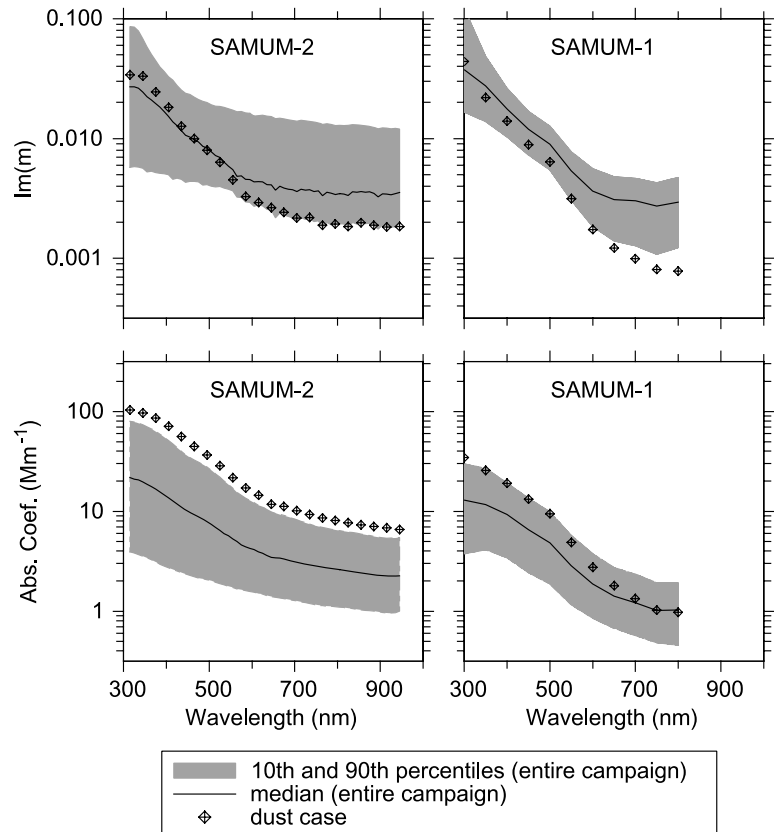


Fig. 8. Measured absorption coefficients and derived imaginary parts of refractive indices for SAMUM-1 and 2. Shown are the medians, 10th and 90th percentile of the entire campaigns. Also typical dust cases (29 January 2008 in case of SAMUM-2) are shown, which are not necessarily periods with the highest dust concentrations.

Ångström exponent of about 1, not shown). During SAMUM-2, a considerable amount of non-absorbing sea salt influenced the observations at the surface (Schladitz et al., 2011a). However, in the wavelength range from 300 to 550 nm the spectral imaginary part of refractive index is comparable to the spectral dependence found during SAMUM-1. This spectral dependence suggests a higher amount of iron in the dust particles over Cape Verde than in southern Morocco. At longer wavelengths the imaginary part of the refractive index differs between both campaigns. These observations points to different origins and mineralogical composition of dust observed during SAMUM-1 and SAMUM-2.

### 3.4. RF studies

Bauer et al. (2011), Köhler et al. (2011) and Torge et al. (2011) deal with the radiative transfer in the atmosphere. Figure 9 emphasizes the impact of the surface albedo on solar RF and corroborates that accurate, spectrally resolved values of surface albedo are needed to assess the impact of dust and smoke on irradiances and, more general, on the Earth's radiative budget. The details of the solar RF calculations using the profile of the particle extinction coefficient and the related particle optical thickness AOT from the parallel HSRL measurements aboard the

Falcon are given by Bauer et al. (2011). The dominant parameter controlling solar RF is the surface albedo. Spectral surface albedo values were determined from airborne spectral upward irradiance measurements. As a specific example, the results of measurement-based simulations of the solar RF are presented for the flight from Cape Verde to Senegal, which was performed in the early afternoon of 29 January 2008. On this day, dust transport in the lowermost 2 km of the troposphere prevailed. Smoke layers above were almost absent. The height-time display of aerosol layering on this day is presented in fig. 3(b) of Knippertz et al. (2011). Compared to the surface albedo effect, the influence of AOT of the desert dust particles on RF is small. The low surface albedo over the Atlantic Ocean leads to negative instantaneous aerosol RF (cooling) with values of  $-18$  to  $-32$   $W m^{-2}$  for AOTs between 0.22 and 0.41.

The RF efficiency (RFE, slope of RF versus aerosol optical depth) plotted in the right panel of Fig. 9 is negative according to the correlation of aerosol RF versus aerosol optical depth. RFE over sea ( $-81$   $W m^{-2}$ ) is much lower than over land ( $-10$   $W m^{-2}$ ). Thus, the solar cooling effect is less pronounced over the more reflective land surface. The impact of the surface albedo on the aerosol solar RF is dominant over land. The slope of the RF curve as a function of AOT can be neglected (see Fig. 9). Therefore, obviously the effect of surface albedo on

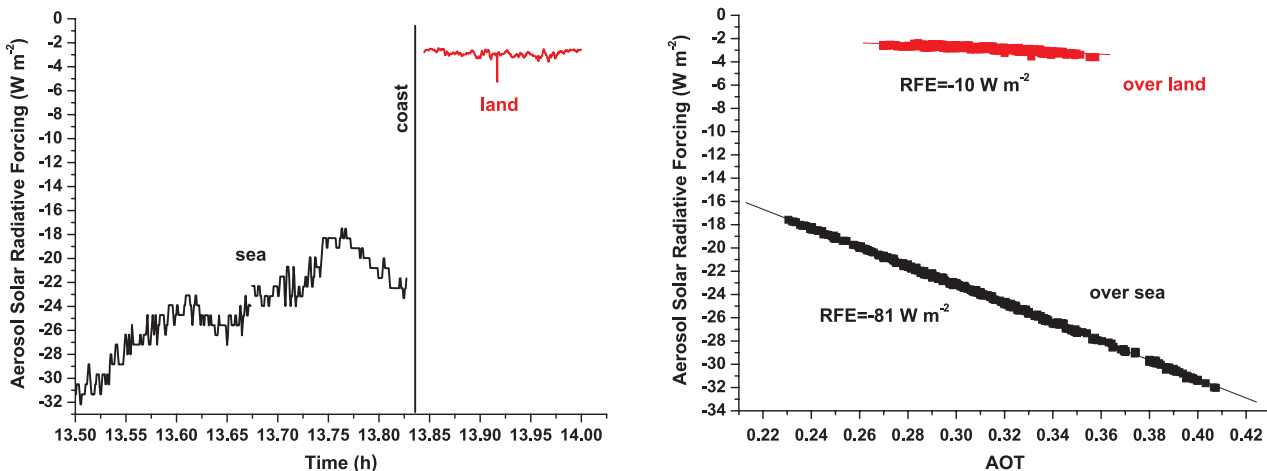


Fig. 9. Aerosol solar radiative forcing as a function of surface albedo (ocean versus continent) and slightly varying aerosol conditions with particle optical thickness (AOT) from 0.22–0.41 at 550 nm (left-hand side) and as a function of AOT separately for flight segments over the tropical North Atlantic and over Senegal in western Africa (right-hand side). Radiative forcing efficiencies (RFE, forcing values for AOT = 1) are given as numbers. The observation is based on radiative flux measurements between Cape Verde and Senegal aboard the Falcon on 29 January 2008, 1330–1400 UTC.

aerosol solar RF is much larger than that of AOT. More details on these studies are given by Bauer et al. (2011) and Tegen et al. (2010) based on SAMUM-1 observations.

Köhler et al. (2011) conducted ground-based spectral downward radiance measurements in the thermal infrared (TIR) and used the SAMUM-consortium data on the optical and microphysical properties of the aerosol particles (particle size, composition, shape and vertical distribution) in radiative transfer calculations. They performed a radiative closure in the TIR based on the ground-based data and, in addition, space-borne high spectral resolution radiance observations. Modelled and measured spectra agree within the estimated error budgets, and the dust-related long-wave direct radiative effect (DRE) in the TIR atmospheric window region (8–12  $\mu\text{m}$ ) is estimated to be 8  $\text{W m}^{-2}$  at the surface and 1  $\text{W m}^{-2}$  at the top of the atmosphere (see also table 4 in Köhler et al., 2011). Their investigations show that the DRE at the surface of the atmosphere is most sensitive to the size distribution and vertical extension of the aerosol layers. The mineral refractive index, surface emissivity and surface temperature seem to have a minor effect here. At the top of the atmosphere, however, surface emissivity and temperature significantly influence the DRE.

Torge et al. (2011) calculated radiative fields of three-dimensional inhomogeneous Saharan dust layers at solar wavelength (0.6  $\mu\text{m}$ ) by means of a Monte Carlo radiative transfer model. The scattering properties for different particle shapes (spheres, spheroids and crystals) are compared. Furthermore, the effect of horizontal photon transport in the simulated radiation fields is studied. This effect can cause significant uncertainties in the order of 10–15% (locally) in cases of strong horizontal AOT gradients or when Sun elevation angle is low and is thus not negligible for these specific conditions. Such investigations are

used to interpret radiance observations with space-borne sensors such as Meteosat Second Generation (MSG).

### 3.5. Regional modelling

During SAMUM-1 the regional dust model version of COSMO-MUSCAT (multiscale atmospheric transport modelling) was developed and used for simulations of the spatiotemporal distribution and radiative effects of Saharan dust (Heinold et al., 2008; 2009; Laurent et al., 2010; Tegen et al., 2010). In SAMUM-2, the regional model was used to study the mixed plume of Saharan dust and biomass-burning aerosol transported off the West African coast towards the Cape Verde area (Heinold et al., 2011a). For this purpose, COSMO-MUSCAT was extended by a scheme for emissions of smoke particles by fires. The model allows for online interaction of the computed aerosol load with the solar and terrestrial radiation, and as one of the first regional aerosol models it includes radiative effects on atmospheric dynamics, aerosol emission and transport. In the case of SAMUM-2, a grid resolution of 28 km is chosen which is a compromise between the possibility to accurately represent dust emission events and the possibility to perform sufficiently long model runs for the large area that must be represented. 40 vertical layers with vertical resolution from 60 m (lower troposphere) to 600 m (upper troposphere) are simulated.

Regional dust and land-fire simulations were performed for the entire period of SAMUM-2. Figure 10 shows the example for 4 February 2008 (evening). At that time, dust advection in the lowermost 1.5 km was weak, lofted dust and smoke plumes dominated. The simulations are compared with corresponding satellite retrieval products. Details of the quality of the comparison with observations is given by Heinold et al.

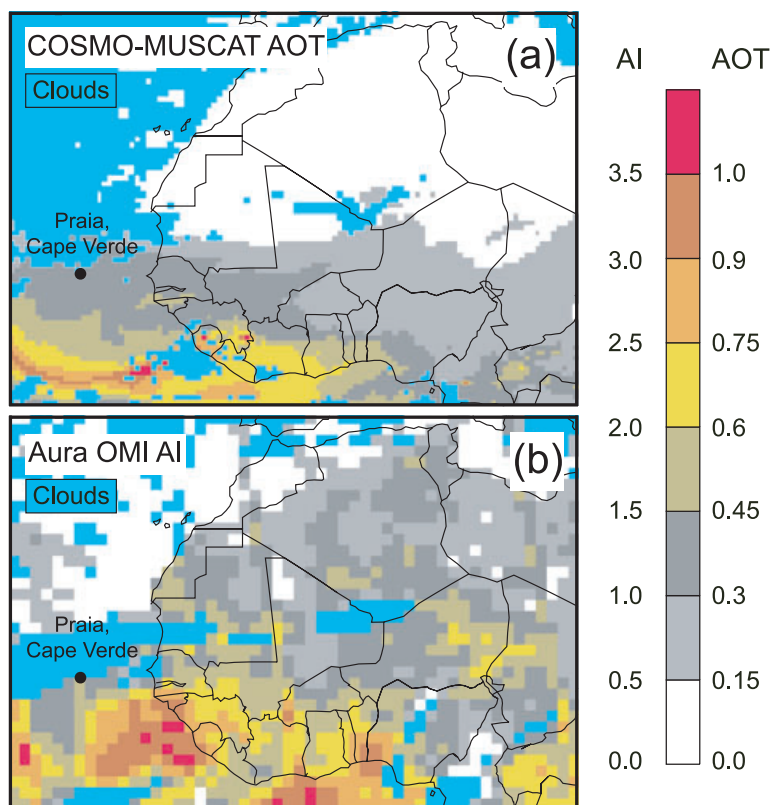


Fig. 10. Maps of the horizontal distribution of Saharan dust and biomass-burning aerosol on 4 February 2008: Particle optical thickness AOT at 550 nm retrieved from (a) model simulations and (b) OMI aerosol index providing semiquantitative information on absorbing aerosol load. Cloudy areas are given in light blue.

(2011a). The modelled spatiotemporal distribution of Saharan dust and biomass-burning smoke was used to study the aerosol radiative effects and feedbacks for different scenarios (Heinold et al., 2011b). The dry synoptic-scale dynamics that cause dust events during the winter season are usually well reproduced by the meteorological model. However, modelled winds and dust distributions were not always reproduced. One reason could be that dust mobilization is influenced by small-scale topography that is not resolved by the model when using a grid scale of 28 km. Over the western part of the Gulf of Guinea the modelled particle optical depth was often lower than the optical depth inferred from satellite observations as the fire maps that are used for model initialization were frequently contaminated by clouds and the simulated Bodélé dust emissions were too low.

In Fig. 11, vertical profiles of smoke and dust obtained with the COSMO model are compared with lidar observations in terms of backscatter coefficients. The simulated dust and smoke number concentrations for different size classes and height layers are transformed into profiles of the extinction coefficient at 532 nm. For the conversion into backscatter coefficients, an extinction-to-backscatter ratio (lidar ratio) of 55 sr (dust) and 70 sr (smoke) is applied. The model resolves the lofted plume of smoke and dust observed with the lidar and roughly depicts the relative contribution of smoke and dust particles to the respective total particle backscatter coefficients (in red in the figure). The height-

integrated (column) backscatter values for the height range from 1.5 to 4.5 km are close to the respective lidar values (for smoke, dust and total particle backscatter). Significant discrepancies between the aerosol layering as modelled and observed occur at greater heights. The vertical resolution of several hundred metres is not sufficient to resolve all the details of aerosol layer structures detected by the lidar. More examples are discussed by Heinold et al. (2011a).

Similar model simulations (separating of dust and smoke) and comparison with respective airborne in situ observations were performed in the framework of DABEX and are discussed by Johnson et al. (2008a) and Myhre et al. (2008). Heinold et al. (2011b) find maximum negative surface forcing of  $-40 \text{ W m}^{-2}$  for the Sahel region, and maximum positive forcing up to  $20 \text{ W m}^{-2}$ , averaged for the same region. The discrepancy in computations of Heinold et al. (2011b) for the SAMUM experiment and Myhre et al. (2008) for the DABEX experiments is mainly related to the SSA assumptions and differences in the aerosol layering structures (dust/smoke aerosol mixtures above the cloud-free or cloudy, polluted, dusty or dust-free marine or continental MBL). Myhre et al. (2008) assumed 550 nm SSA values of 0.73 or 0.81 for smoke, and 0.98 for dust, whereas Heinold et al. (2011b) used values of 0.52 (250–700 nm) and 0.45 (700–1530 nm) for smoke and 0.79 (250–700 nm) and 0.98 (700–1530 nm) for dust (see Heinold et al., 2011b, for more details). The effect of including RF in the regional model led

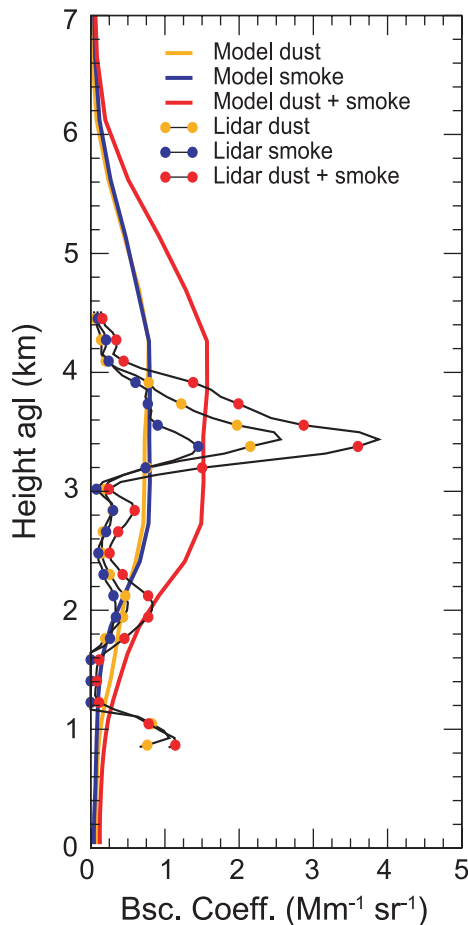


Fig. 11. Comparison of modelled (solid coloured lines) with respective observed (lidar, black lines with coloured circles) profiles of dust (orange), smoke (blue) and total particle (red) backscatter coefficient (532 nm). The lidar measurement was performed in the evening of 4 February 2008.

to an enhancement of the Hadley circulation and a better representation of the smoke layers compared to neglecting those radiative effects. Given the choice of very low SSAs for smoke aerosol these radiative effects have to be considered as maximum effects.

#### 4. SAMUM-1 and SAMUM-2 highlights and main findings: what have we learned?

In this section we summarize the SAMUM activities and results. This is done separately for in situ observations of microphysical, chemical and optical properties at ground and aboard the Falcon (Table 3), remote sensing with lidars and photometers (Table 4), radiative transfer studies (Table 5), and regional dust modelling (Table 6).

From the point of view of the in situ characterization of dust (Table 3) the most contrasting feature with respect to previous

field observations was the airborne measurement of the particle size distribution up to very large particles with diameters of 100  $\mu\text{m}$  (SAMUM-1, Weinzierl et al., 2009) and the determination of the spectral absorption coefficient of desert dust particles (Müller et al., 2009b; 2011). The comprehensive efforts to study the chemical, mineralogical and morphological properties of the sampled aerosol particles must also be emphasized (Kandler et al., 2009; 2011a; 2011b; Lieke et al., 2011; Scheuvs et al., 2011). In contrast to previous field work the imaginary part of the dust refractive index was determined from various methods including chemical composition, absorption photometry and inversion methods. A variety of closure studies shows the consistency and quality of the different measurements (e.g. Müller et al., 2010a; 2011).

In the case of active remote sensing, the most contrasting feature to previous campaigns was the unique aerosol lidar facility. A Doppler lidar for vertical mixing studies and the HSRL aboard the Falcon completed the SAMUM lidar instrumentation. The TSP/PM<sub>10</sub> ratios of 1.25 (SAMUM-2) and 8–9 to 35–40 (SAMUM-1) presented in Table 4 corroborate the importance of extinction profiling at ambient conditions. A considerable part of large particles (causing large optical effects) are missing in surface and airborne in situ observations of optical and microphysical properties when PM<sub>10</sub> inlets are used only.

The highlights of the lidar activities and the main findings are presented in Table 4. The lidar products and the SAMUM photometer results of Toledano et al. (2009, 2011) and von Hoyningen-Huene et al. (2009) were used in a variety of SAMUM closure and transport modelling studies and verification of passive remote sensing from space (Dinter et al., 2009; Kahn et al., 2009). They served as benchmark data in tests of scattering models for non-spherical dust particles and in CALIPSO ground truth activities, and triggered the development of new lidar-based schemes for the separation of the optical properties of dust and non-dust (i.e. smoke in the case of SAMUM-2) particles and the subsequent retrieval of the smoke-related microphysical properties and SSA. The closure studies regarding SSA (remote sensing versus in situ observations) separately for dust and smoke are one of the strong points of the SAMUM-2 efforts. The combination of airborne lidar and in situ observations enabled us to introduce a new approach to characterize the aerosol type (smoke, dust, marine particles and mixtures of these basic aerosol types) by combining the depolarization ratio, lidar ratio and absorption Ångström exponent information (Weinzierl et al., 2011).

The validation study regarding AERONET dust products based on the comparison of diverse dust parameters from surface, Falcon and lidar observations with respective retrieval results of AERONET Sun photometer observations during SAMUM-1 (pure dust cases) is an essential highlight and marks considerable progress for the global aerosol community. This effort can be regarded as the most comprehensive and complex SAMUM closure study and is described in detail by Müller et al. (2010a,b).

Table 3. Selected efforts and results of in situ measurements of microphysical, optical and chemical properties during SAMUM-1 and SAMUM-2.

**Chemical/mineralogical analysis products**

- Surface measurement of bulk-mineralogical composition: SAMUM-1 (quartz 24–67%, K-feldspar 10–25%, illite 5–10%, other silicates 3–8%, calcite 1–3% and hematite 1–2%), SAMUM-2 (kaolinite 35%, K-feldspar 20%, illite 14%, quartz 11%, smectite 6%, plagioclase 6%, gypsum 4%, halite 2% and calcite 2%) (Kandler et al., 2009; 2011a; Lieke et al., 2011).
- Determination of individual particle shape for fresh and aged dust: Aspect ratio (length-to-width ratio) of 1.6 for particles with  $D > 500$  nm, values towards 1.3 for dust particles with  $D = 100$  nm, slight dependence of average aspect ratio (length-to-width ratio) on particle chemistry (Kandler et al., 2007; 2009; 2011b; Scheuvs et al., 2011).
- Modelling of refractive indices from chemical composition, mineral dust mean value: Real part of 1.57, imaginary part of 0.0037 at 530 nm for particles with  $D > 500$  nm. Determination of the imaginary part as function of particle size for aerosol dominated by soot, dust, non-absorbing particles (Kandler et al., 2009; 2011b; Lieke et al., 2011; Schladitz et al., 2011a).

**Microphysical characteristics**

- Determination of particle mass concentrations: Significantly more large particles on the African continent (TSP/PM10 = 8–9 during background, 35–40 during high wind conditions) than at Cape Verde (TSP/PM10 = 1.25) (Kandler et al., 2009; 2011a).
- Airborne measurement of the entire dust size distribution from the nucleation mode to the far super-micron range ( $4 \text{ nm} < D < 100 \text{ }\mu\text{m}$ , SAMUM-1,  $4 \text{ nm} < D < 30 \text{ }\mu\text{m}$ , SAMUM-2, Petzold et al., 2011; Weinzierl et al., 2009; Weinzierl et al., 2011): During SAMUM-1, in all cases particles with  $D > 10 \text{ }\mu\text{m}$  were present, and in most cases (80%)  $D < 40 \text{ }\mu\text{m}$  (Weinzierl et al., 2009). In contrast, no particles with  $D$  around  $30 \text{ }\mu\text{m}$  were found during SAMUM-2 and in several cases even no particles with  $D > 10 \text{ }\mu\text{m}$  were detected (Weinzierl et al., 2011). During SAMUM-2 biomass-burning aerosol was observed in an elevated accumulation-mode size range of  $0.1\text{--}1.0 \text{ }\mu\text{m}$ , the mineral dust mode was always present in the biomass-burning plumes (Weinzierl et al., 2009; 2011).
- Determination of the hygroscopic behaviour of mineral dust and mixtures (e.g. dust/marine) (Kaden et al., 2009; Schladitz et al., 2011a). Saharan dust particles observed during SAMUM-1 and SAMUM-2 were almost non-hygroscopic (Schladitz et al., 2011b).

**Optical properties**

- Determination of the spectral absorption coefficient of dust particles and the imaginary part of the refractive index by spectral absorption photometry and by an inversion method (Petzold et al., 2009, 2011; Müller et al., 2009b, 2011; Weinzierl et al., 2011): Dust refractive index, imaginary part (pure dust), 0.0051 (450 nm), 0.0016 (550 nm), 0.00045 (650 nm) (Müller et al., 2009b). Similar spectral dependencies were found for SAMUM-1 and SAMUM-2 at ground (see fig. 8, Müller et al. (2011)).
- Values of the absorption Ångström exponent ranged from 1.0 in anthropogenic pollution plumes and biomass-burning layers to  $>5$  in pure dust layers (Petzold et al., 2009, 2011, Müller et al., 2009b; 2011; Weinzierl et al., 2011).
- SSA: 0.96 (537 nm), 0.98 (637 nm) (Schladitz et al., 2009), 0.91 (450 nm), 0.96 (550 nm), 0.98 (950 nm) (Müller et al., 2011). Airborne values of SSA for dust cases: 0.96–0.99 (530 nm,  $D < 3 \text{ }\mu\text{m}$ ) (Petzold et al., 2011).

Note: PM10 denotes particulate matter with aerodynamic diameter  $D_a < 10 \text{ }\mu\text{m}$  and TSP stands for total suspended particle mass.

For the lidar community, most important are the measured pure-dust extinction-to-backscatter and depolarization ratios. Such observations are hard to achieve over polluted continents. Modelling of lidar-related optical properties of mineral dust was notably improved by assuming irregularly shaped particles and mixtures of absorbing and non-absorbing model particles (Gasteiger et al., 2011). Irregularly shaped particles (partly deviating in shape from the spheroidal form by introducing surface roughness) improve the agreement of modelled with the observed linear depolarization ratios. Mixtures of absorbing and non-absorbing particles are essential to reproduce the observed spectral change of the lidar ratio.

Table 5 summarizes the main findings regarding the efforts to characterize the impact of Saharan dust on the Earth's radiation budget. The first half of the table covers SAMUM-1 activities, the second half describes the results of SAMUM-2. In SAMUM-1 typical spectral signatures of surface albedo over different surface types in Morocco were derived. It was shown that the spectral surface albedo exerts a major influence on the upwelling spectral irradiances and radiances. The surface

albedo impact is comparable to the effects caused by the optical properties of the aerosol particles (mainly optical thickness). SAMUM-2 showed that over sea the surface albedo is of less importance for the upward radiation in the solar spectral range.

From measurements of downward TIR during SAMUM-2, spectral radiance in the window region the effect of dust particles on terrestrial radiation was estimated. The total DRE at the top of the atmosphere is small compared to one at the surface because the dust layers of dominant optical depth were located close to the surface during SAMUM-2, which results in temperatures similar to those of the surface and thus only small differences between absorbed and emitted radiation. Furthermore the examinations of Köhler et al. (2011) revealed that absorption and emission are dominating radiative transfer processes in the TIR compared to scattering, which seems to have a minor influence on the simulated spectra.

A major strength of the SAMUM project was the close interaction between projects involving field and laboratory measurements, and the development and application of the regional dust models (Table 6). Based on existing model components, the

*Table 4.* Important lidar activities, new approaches and some key lidar and photometer findings based on SAMUM-1, SAMUM-2a (winter campaign) and SAMUM-2b (summer campaign).

---

#### Profiling of pure dust optical properties (at ambient conditions)

- Dust extinction coefficient (532 nm):  $90 \pm 60 \text{ Mm}^{-1}$  (SAMUM-1 mean and standard deviation, 2–4 km height agl, Tesche et al., 2009a),  $140 \pm 160 \text{ Mm}^{-1}$  (SAMUM-2a, 0.5–1.3 km height agl, Groß et al., 2011a),  $20 \pm 20 \text{ Mm}^{-1}$  (SAMUM-2a, dust only, 2–4 km height agl),  $80 \pm 60 \text{ Mm}^{-1}$  (SAMUM-2b, 2–4 km height agl, Tesche et al., 2011a).
- Dust linear depolarization ratio: 0.22–0.27 (355 nm), 0.27–0.35 (532 nm), 0.30–0.42 (710 nm) (Freudenthaler et al., 2009; Groß et al., 2011a).
- Dust lidar ratio (355 nm, 532 nm, 1064 nm): 50–60 sr (Tesche et al., 2009a; 2011a; Groß et al., 2011a; b).

#### Profiling of dust in mixed aerosol plumes

- Separation of dust and smoke (Tesche et al. 2009b; 2011b), smoke-related SSA (532–nm): 0.65–0.9, lidar ratio: 60–100 sr.
- Aerosol typing based on depolarization and lidar ratios (Groß et al., 2011b), and, in addition, on in-situ-measured absorption Ångström exponents (Weinzierl et al., 2011).

#### Unique opportunities for comparison (pure mineral dust)

- Modelling: Simulation of shape-dependent scattering properties (depolarization ratio, lidar ratio), testing of a variety of new shape models (Wiegner et al., 2009; Gasteiger et al., 2011). Mixtures of non-absorbing and absorbing dust particles are essential to reproduce the spectral changes of the measured lidar ratios, irregular particles (deviating from the spheroidal form) are required to reproduce the measured depolarization ratios.
- CALIPSO: Comparison of dust profiles from SAMUM and CALIPSO lidar observations, analysis reveals that CALIPSO underestimates the dust optical depth by about 25% caused by neglected multiple scattering (Wandinger et al., 2010).
- AERONET: Comprehensive comparisons of AERONET products with respective SAMUM-1 observations (lidar, photometer, in situ) for pure dust (Müller et al., 2010a; b). Good agreement in the case of particle extinction (optical depth) and Ångström exponent. Significant difference between the AERONET particle size distributions and airborne in situ measurements of the coarse mode fraction. Particle scattering and particle absorption do not match regarding their spectral behaviour. Dust properties describing absorption at near ultraviolet wavelengths are lower (complex refractive index) respectively higher (lidar ratio, SSA) from AERONET compared to lidar observations and in situ characterization. Dust depolarization ratios from AERONET are lower than the ones measured here. Further studies for complex aerosol mixtures during SAMUM-2 are presented by Toledano et al. (2011).

#### Vertical exchange studies

- Profiling of dust devils and convective plumes (for the first time), important feature: dust injection occurs at low mean wind ( $< 7 \text{ m s}^{-1}$ ) conditions (Ansmann et al., 2009a).
  - Vertical-wind profiling to study heat island effects on downward mixing of aerosols towards the ocean surface, strong disturbance of the air flow around and over the island was found (Engelmann et al., 2011; Weinzierl et al., 2011).
- 

new model design includes dust and smoke aerosol as radiatively active components of the atmosphere. This setup allowed us to test the impact of changes in boundary layer stability and atmospheric dynamics by the absorbing aerosol particles (Heinold et al., 2007; 2011b; Helmert et al., 2007). A horizontal model grid resolution of 28 km was found to be appropriate to simulate most relevant processes of dust production, transport and radiative effects. However, dust processes related to wet convective events were better represented at grid resolution of 2.8 km (Heinold et al., 2009; Reinfried et al., 2009).

The possibility of a direct evaluation of aerosol concentrations and vertical distribution, microphysical properties and radiation measurements offered unique opportunities for model evaluation near and downwind of source regions. In this sense the regional dust model provided a test bed to evaluate under which conditions the model results matched the observations well, and when they failed. In this context the model results were used as a starting point for evaluating the parameterization of soil properties important for dust emission (Laurent et al., 2010), and of specific processes of dust production such as the observed dust mobilization by density currents (Knippertz et al., 2007; 2009).

The impact of boundary layer processes on dust distribution, and in turn the dust RF impact on boundary layer stability was explored with this model system, showing that the instantaneous effects of dust RF on dust emission can be positive under certain circumstances (Heinold et al., 2008).

Extending the model to include smoke aerosol forcing as part of SAMUM-2 allowed us to investigate dust and smoke radiative effects (Heinold et al., 2011a). The SAMUM model studies highlight the importance of evaluating the dust simulations separately for different types of dust events. A novel compilation of dust source activation events based on infrared geostationary satellite measurements revealed the importance of processes of dust mobilization which occur in the morning hours. Turbulent downward mixing of momentum during the breakdown of the nocturnal low level jet causes this dust mobilization (Schepanski et al., 2007; 2009). Even at grid resolution of 28 km the model was well capable of reproducing such events. The results for other dust activation events involving wet convection were improved with grid resolution of at least 2.8 km (Knippertz et al., 2009; Reinfried et al., 2009). However, such high resolution could only be realized for few individual events.

Table 5. Essential results from radiation studies.

**SAMUM-1**

- Airborne observations of surface albedo, mostly around 0.1 at 500 nm, up to 0.2 at 1–2  $\mu\text{m}$  wavelength in most desert areas of southern Morocco, and up to 0.5 over salt lakes (Bierwirth 2008; 2009).
- Spectral RF of Saharan dust is equally dependent on both the underlying surface albedo and the optical properties of the dust (in particular of the SSA). The influence of the asymmetry parameter is comparable to that of the SSA, its influence is reduced over bright surfaces.
- The broad-band solar RF (top-of-atmosphere) increases by up to  $12 \text{ W m}^{-2}$  for a surface-albedo increase of 0.1. The influence decreases at higher dust loads, but is also modified by the vertical profile and the optical properties of the dust.
- Total instantaneous RF of the observed Saharan dust ranged between  $-22$  and  $-42 \text{ W m}^{-2}$  at the surface, and between 0 and  $22 \text{ W m}^{-2}$  at top of atmosphere. It would be negative over dark surfaces such as the ocean.
- Development of a new method to combine airborne radiation measurements of irradiance and actinic flux density to derive the absorption coefficient of an aerosol layer (Bierwirth et al., 2010).
- Significant differences (10–20% at top and bottom of the atmosphere) in solar and thermal radiative transfer calculations when considering more realistic dust particle shapes (spheroidal instead of spherical shape), more realistic aspect ratios (size-dependent versus size-independent), and refractive index characteristics (from SAMUM-1 observations, Otto et al., 2009; 2010).

**SAMUM-2**

- Airborne observations of upward radiance and irradiance in the solar wavelength range over sea and over land together with the particle extinction coefficient profile for a variety of different aerosol mixtures from pure dust to almost pure smoke (Bauer et al., 2011).
- During a land–sea overflight a significant increase of negative solar RF from about  $-3 \text{ W m}^{-2}$  over land to  $-20 \text{ W m}^{-2}$  to  $-30 \text{ W m}^{-2}$  over sea was observed.
- Determination of the solar RF efficiency as a function of the surface albedo (Otto et al., 2011; Bauer et al., 2011).
- Ground-based high spectral resolution measurements of downward radiances in the 8–12  $\mu\text{m}$  atmospheric window region, the mixed Saharan dust/biomass-burning aerosol has a distinct effect on the downward spectral radiation in the TIR window region and amounts to a DRE of  $8 \text{ W m}^{-2}$  at the surface and  $1 \text{ W m}^{-2}$  at the top of the atmosphere (Köhler et al., 2011).
- Radiative effects in the TIR window region due to the aerosols as observed during SAMUM-2 seem to be caused by emission and absorption processes, whereas scattering plays a minor role.

Table 6. SAMUM milestones from the modelling point of view.

**SAMUM-1**

- Development and evaluation of a regional-scale Saharan dust model. Dust particles interact with radiative transfer in the solar and thermal wavelength ranges (Heinold et al., 2007; Helmert et al., 2007).
- Use of soil texture and soil grain size information from geomorphological analysis and soil samples improved the model performance (Laurent et al., 2010).
- MSG imagery shows that dust emissions occur preferentially in the vicinity of mountain slopes rather than in flat, smooth terrain. The MSG data established the important role of the break-down of nocturnal low-level jets for the number of Saharan dust source activations (Schepanski et al., 2007; 2009).
- Different convection parameterization schemes and model resolutions tested, most realistic representation of dust emission events related to wet convective activity is obtained at 2.8 km grid resolution (Knippertz et al., 2009; Reinfried et al., 2009), but as standard 28 km grid resolution is used.
- In the regional average over the Sahara the modelled diurnal mean solar top-of-atmosphere RF by dust ranges between  $-1.7$  and  $-9.4 \text{ W m}^{-2}$  for a typical dust day (19 May 2006, optical depth of 0.4), depending on dust optical properties and surface albedo (Tegen et al., 2010). In the regional average over the Sahara using either the standard model values or satellite-based surface albedo values leads to differences in the order of  $5 \text{ W m}^{-2}$  for the diurnal mean TOA forcing. Instantaneous forcing of dust can be positive and up to  $11 \text{ W m}^{-2}$ .
- Feedback of dust RF upon dust emission and transport can reduce modelled dust optical thicknesses locally by 40–70%. Over the total SAMUM-1 period the reduction is 3–4% averaged over the cloud-free Sahara and 5% over the Bodélé (Heinold et al., 2008).

**SAMUM-2**

- Model results capture the complex layering of mineral dust and biomass-burning smoke transported off the West African continent (Heinold et al., 2011a).
- Radiative impact of dust and smoke leads to the local modification of air-flow patterns (Hadley circulation is enhanced), comparisons with lidar measurements show that the vertical distribution of smoke aerosol is more realistic when its radiative impact is considered (Heinold et al., 2011b).

Measurements during SAMUM allowed us to constrain Saharan dust optical properties near and downwind of the source regions. The modelling results allowed us to assess the remaining RF uncertainty. We found that the dust forcing uncertainty is on the same order of magnitude as the uncertainty in surface albedo as prescribed in the model (Bierwirth et al., 2009; Tegen et al., 2010). The project also offered the opportunity to study the role of parameterization of wet versus dry deposition in the model. As a result of SAMUM, the dust version of the regional model system COSMO–MUSCAT has become a useful tool to study processes of atmospheric dust transport and effects, and to provide a spatiotemporal context to field studies dedicated to Saharan dust. The main steps forward reached in the framework of the SAMUM project are summarized in Table 6.

## 5. Open questions and outlook

SAMUM made substantial efforts combining different instruments of optical and microphysical dust properties and data analysis methodologies. Yet there remain in part significant differences for some of the data products. For instance we cannot achieve a satisfactory reproduction of the particle depolarization ratio and the lidar ratio, measured with lidar and modelled from AERONET Sun photometer observations (Müller et al., 2010b). We emphasize that the modelling of the optical properties of mineral dust at  $180^\circ$  is particularly challenging as the particle shape has significant impact on the optical properties at this scattering angle. The AERONET algorithm was never designed for such specific scattering geometries. However, in order to improve methodologies of remote sensing of dust, any future light-scattering model used for the description of optical and microphysical properties of dust must include extreme backward scattering. Such models will particularly be needed for the inversion of lidar data, and when combining data collected with lidar and passive remote sensors into microphysical parameters of dust.

The lack of accurate methods for irregularly shaped particles with size parameters much larger than 20 is another critical point of optical modelling of dust aerosols. More modelling (sensitivity) studies based on a variety but realistic dust particle shapes (deviating from the ideal spheroidal shape) are required. The distribution of the absorbing material within the particles and the consequences for the optical properties need to be investigated.

The modelling of light absorption on the basis of measured particle size distributions and complex refractive indices (inferred from the chemical analysis of dust particles) leads to gross differences to light absorption inferred from the inversion of remote sensing data, in particular at ultraviolet wavelengths (Müller et al., 2010a). We need continuing improvements in techniques for measuring the wavelength-dependent optical properties of dust. Kandler et al. (2009, 2011b) show that parameters like the imaginary part can be inferred from measurements of particle chemical composition. However, the mixing rules that

are used to derive the volume-averaged complex refractive index from the complex refractive indices of the individual components of dust are still not verified by independent measurement methodologies. This is especially true for the TIR region where resonance features in the real and complex part of the refractive index of mineral dust compounds are of key importance for simulating the spectral signature of dust. A direct proof is at least possible with the absorption photometer in the case of the solar spectrum (Müller et al., 2009b; 2011).

There remains the question of accurate measurements/retrievals of particles in the coarse mode of the size distribution. These particles are essential for radiative dust properties. In situ observations in general lead to considerably larger mean particle sizes than what was inferred from remote sensing instrumentation during SAMUM. The uncertainties in the in situ observations can be large and must be accurately quantified. New techniques may be introduced to measure large to giant non-spherical aerosol particles. The open question in the remote sensing field is whether the geometrical description of particle shape in remote sensing methodologies must be further improved, whether the inaccurate retrievals are a combination of many different factors like (1) particle shape, (2) limited optical information in remote sensing instruments, (3) assumptions and constraints that are made in the analysis of the remote sensing signals (as for instance the inversion from optical into microphysical properties) and (4) particle morphology information. Concerning point (2) we need to expand our measurement wavelength range. Optical particle properties in the infrared cannot be extrapolated from data in the wavelength range from 440–1020 nm. Sun photometers downwind of regions of dust emission and transport need to be equipped with a channel at 1640 nm, and the operational inversion schemes applied to retrieve microphysical dust properties must include the long-wavelength channel information which is not the case yet. Additional channels extending the wavelength range to five or even 10  $\mu\text{m}$  such as utilized by Grassl (1970) already would be preferable. Such an expansion of measurement wavelengths, however, should not be restricted to Sun photometers only. An expansion of lidar profiling to 1  $\mu\text{m}$  wavelength and beyond would greatly advance our understanding of light absorption of dust in the atmosphere.

For the interpretation of remote sensing measurements and to provide input for aerosol models, we need laboratory studies that focus on improved complex refractive index measurements of pure mineral dust and mixtures of dust, for example, with non-absorbing materials like sea salt, with low absorbing particles, like sulphates, and with strongly absorbing materials like soot. We need more size-resolved information on particle morphology under ambient atmospheric conditions. In that regard, however, not only particle measurement methodologies must be further improved; a more straightforward mathematical description of particle shape and how to include it into dust remote sensing methods must be found. At the moment the methods basically

rest upon the scanning of two-dimensional (projected) shapes, regardless of the fact that dust particles have a complicated three-dimensional structure. Finally we may in the end be forced to use a combination of different remote sensing methodologies like lidar and Sun photometer plus additional instruments in order to infer dust properties with satisfying accuracy. SAMUM in that respect has demonstrated several options, which need to be further investigated in future.

The determination of SSA of mineral dust remains one of the key questions to be addressed further. The SAMUM results indicate that the observed discrepancy between values from remote sensing techniques and values derived from in-situ-measured size distributions may be associated with the different dust particle size ranges that are considered in the different approaches. However, the direct measurement of the dust SSA at different wavelengths is the missing link in terms of the dust impact on climate. Investigations of SSA of smoke (freshly emitted versus aged, long-range transported smoke originating from smoldering or burning fires) remain necessary for further field studies.

The SAMUM campaigns like the earlier DABEX and DODO field experiments point to the importance of further studies (observations and modelling) on mixtures of aerosols and the impact of aerosol layer structures (smoke layer above dust layer, dust/smoke layer above cloud-free or cloudy MBL, etc.) on solar and terrestrial upward and downward radiative fluxes. In addition, these complex aerosol scenarios affect cloud evolution processes, and probably in very different ways.

First studies of regional-scale transport events during SAMUM-1 (Wagner et al., 2009), observations during PRIDE in Puerto Rico (Maring et al., 2003) as well as transport studies of large radioactive particles (Persson et al., 1987), show that even large super-micrometre dust particles are transported over long distances. The identification of meteorological processes during long-range transport, which keeps super-micrometre dust particles airborne is still an open topic and is subject to ongoing work based on SAMUM data. On the other hand, the effect of particle sedimentation became obvious in the SAMUM-2 data when compared with the SAMUM-1 data (size distributions). Field experiments significantly further to the west are required to better clarify the role of gravitational settling and also of dust removal by turbulent downward mixing at the top of the MBL. Ship cruises with aerosol/cloud and Doppler lidars from the Cape Verde to the Caribbean islands would be helpful.

The influence of lofted mineral dust layers on atmospheric stability and cloud formation requires dedicated field studies combined with cloud-resolving modelling. This interaction and the involved processes may make a significant contribution to the climate impact of mineral dust.

Saharan dust emission processes were not explicitly studied during SAMUM. However, since direct measurements of dust emission fluxes are impossible, those processes need to be well understood for model studies of dust transport and interactions with meteorology and climate. Saharan dust emission modelling

remains hampered by two main open issues: On the one hand, the description of soil properties including soil particle size distribution, surface crusting and surface roughness is often impossible for Saharan dust sources due to the inaccessibility to source regions. On the other hand, some of the meteorological conditions causing dust emission, in particular small-scale processes involving convection or turbulence, are insufficiently reproduced in models. Whereas sufficiently high model resolution that eliminates the need for parameterization of wet convection improves the model performance in some cases, appropriate subgrid scale parameterizations for surface wind speeds are needed to reproduce spatiotemporal distributions of dust emission for typical dust storm situations. This is especially important for global-scale simulations of mineral dust and its climate interactions. The problem of correct placement of dust emissions has also consequences for matching dust properties measured at remote locations to particular dust source regions.

Although quantification of the correct spatiotemporal distribution of dust emissions is of critical importance for characterizing atmospheric dust loads and their effects, these are also strongly influenced by deposition processes. Particularly wet deposition is an important controlling of the atmospheric dust content in remote regions, but deposition processes in models are only roughly parameterized.

Ageing of dust particle surfaces by mixing with other atmospheric species and/or cloud processing was almost not observed during SAMUM, partly due to the proximity to the dust source regions even at Cape Verde. Such mixing processes also need to be characterized to clarify the role of dust as cloud condensation nuclei for water and ice clouds, as well as characterizing possible changes in the optical particle properties by surface modification. For example, particle modifications by mixing processes need to be studied for cases of long-range transport.

The direct RF of Saharan dust was studied during the SAMUM cases, and its role for modifying atmospheric dynamics over land including the impact of dust forcing on dust emissions was recognized. However, whereas the regional scale of the model studies allowed studying the dust effect on meteorological processes, the sea surface temperatures were held fixed in the model. At larger scales, the role of dust forcing on tropical meteorology needs to consider changes in ocean surface temperature too, which will require climate model studies at high resolution, that take into account the SAMUM results. This will also be a pre-requisite for projections of future changes in Saharan dust forcing and effects that are at least to some degree credible.

## 6. Summary

The present introduction summarizes strategy, design and major findings of the two field campaigns of the SAMUM experiment, the first of which focused on Saharan dust near its source whereas the second campaign studied the dust further away

from its source and interspersed with marine particles and with biomass-burning smoke. Based on the SAMUM experiences, open questions were discussed. Future field campaigns may focus, again, on the dust source regions to cover dust emission issues, and on the far range of the long-range transport regime towards North America in summer and South America in winter. Future field campaigns should also focus on the effects of dust and smoke particles on cloud evolution and formation of precipitation in the intertropical convergence zone over the tropical Atlantic.

## 7. Acknowledgments

We are deeply indebted to Colonel Antonio Fortes whose efforts in overcoming logistical and organizational problems of any kind were the key to our successful campaign. We express our deepest gratitude to the airport authority of the Republic of Cape Verde. We particularly want to thank the director of Praia airport Dr Euridice Mascarenhas and her staff for the warm welcome offered to our science team. Dr Mascarenhas supported us in a non-bureaucratic manner, which made our work at Praia airport very pleasant and successful. We would like to acknowledge the great help we received by the airport staff members Mr Daniel Lima and Mr Antonio Pinheiro. We thank the AERONET team for providing us with the travel version of a well-calibrated AERONET (Cimel) Sun photometer during SAMUM–2. We are grateful to the DLR Flight Operations for their excellent support during the preparation of the field study and during the research flights. The SAMUM research group was funded by the Deutsche Forschungsgemeinschaft (DFG) under grant number FOR 539. We furthermore thank the Johannes Gutenberg University Mainz for its financial support through the research funds of the University of Mainz. The European Space Agency funded SAMUM data analysis with focus on space-borne applications in the framework of the ICAROHS project (contract number 22169/08/NL/CT). We are grateful to DLR for sponsoring about 50% of all SAMUM–2 Falcon flights.

## References

- Andreae, M. O. and Gelencsér, A. 2006. Black carbon or brown carbon? The nature of light-absorbing carbonaceous aerosols. *Atmos. Chem. Phys.* **6**, 3131–3148.
- Ansmann, A., Wandinger, U., Wiedensohler, A. and Leiterer, U. 2002. Lindenberg Aerosol Characterization Experiment 1998 (LACE 98): overview. *J. Geophys. Res.* **107**, 8129, doi:10.1029/2000JD000233.
- Ansmann, A., Bösenberg, J., Chaikovskiy, A., Comerón, A., Eckhardt, S. and co-authors. 2003. Long-range transport of Saharan dust to northern Europe: the 11–16 October 2001 outbreak observed with EARLINET. *J. Geophys. Res.* **108**, 4783, doi:10.1029/2003JD003757.
- Ansmann, A., Tesche, M., Althausen, D., Müller, D., Freudenthaler, V. and co-authors. 2008. Influence of Saharan dust on cloud glaciation in southern Morocco during SAMUM. *J. Geophys. Res.* **113**, D04210, doi:10.1029/2007JD008785.
- Ansmann, A., Tesche, M., Knippertz, P., Bierwirth, E., Althausen, D. and co-authors. 2009a. Vertical profiling of convective dust plumes in southern Morocco during SAMUM. *Tellus* **61B**, 340–353.
- Ansmann, A., Baars, H., Tesche, M., Müller, D., Althausen, D. and co-authors. 2009b. Dust and smoke transport from Africa to South America: lidar profiling over Cape Verde and the Amazon rainforest. *Geophys. Res. Lett.* **36**, L11802, doi:10.1029/2009GL037923.
- Ansmann, A., Tesche, M., Seifert, P., Althausen, D., Engelmann, R. and co-authors. 2009c. Evolution of the ice phase in tropical altocumulus: SAMUM lidar observations over Cape Verde. *J. Geophys. Res.* **114**, D17208, doi:10.1029/2008JD011659.
- Bates, T. S., Huebert, B. J., Gras, J. L., Griffiths, F. B. and Durkee, P. A. 1998. International Global Atmospheric Chemistry (IGAC) project's First Aerosol Characterization Experiment (ACE 1): overview. *J. Geophys. Res.* **103**, D13, doi:10.1029/97JD03741.
- Bauer, S., Bierwirth, E., Esselborn, M., Petzold, A., Macke, A. and co-authors. 2011. Airborne spectral radiation measurements to derive solar radiative forcing of Saharan dust mixed with biomass burning smoke particles. *Tellus* **63B**, this issue.
- Ben-Ami, Y., Koren, I., Rudich, Y., Artaxo, P., Martin, S. T. and co-authors. 2010. Transport of North African dust from the Bodélé depression to the Amazon Basin: a case study. *Atmos. Chem. Phys.* **10**, 7533–7544.
- Bergametti, G., Gomes, L., Remoudaki, E., Desbois, M., Martin, D. and co-authors. 1989. Present transport and deposition patterns of African dusts to the north–western Mediterranean. In: *Palaeoclimatology and Palaeometeorology: Modern and Past Patterns of Global Atmospheric Transport*. 282, (eds M. Leinen and M. Sarnthelm). NATO ASI Series, C, Kluwer Academic Publishers B.V., Dordrecht, The Netherlands, 227–252.
- Bierwirth, E., 2008. *Airborne measurements of the spectral surface albedo over Morocco and its influence on the radiative forcing of Saharan dust*. PhD Thesis, Johannes Gutenberg-Universität Mainz, Germany.
- Bierwirth, E., Wendisch, M., Ehrlich, A., Heese, B., Tesche, M. and co-authors. 2009. Spectral surface albedo over Morocco and its impact on the radiative forcing of Saharan dust. *Tellus* **61B**, 252–269.
- Bierwirth, E., Wendisch, M., Jäkel, E., Ehrlich, A., Schmidt, K. S. and co-authors. 2010. A new method to retrieve the aerosol layer absorption coefficient from airborne flux density and actinic radiation measurements. *J. Geophys. Res.* **115**, D14211, doi:10.1029/2009JD013636.
- Biscaye, P. E., Grousset, F. E., Revel, M., van der Gaast, S., Zielinski, G. A. and co-authors. 1997. Asian provenance of glacial dust (stage 2) in the Greenland Ice Sheet Project 2 Ice Core, Summit, Greenland. *J. Geophys. Res.* **102**, doi:10.1029/97JC01249.
- Capes, G., Johnson, B., McFiggans, G., Williams, P. I., Haywood, J. and co-authors. 2008. Aging of biomass burning aerosols over West Africa: aircraft measurements of chemical composition, microphysical properties, and emission ratios. *J. Geophys. Res.* **113**, D00C15, doi:10.1029/2008JD009845.
- Chen, G., Ziemba, L. D., Chu, D. A., Thornhill, K. L., Schuster, G. L. and co-authors. 2010. Observations of Saharan dust microphysical and optical properties from the Eastern Atlantic during NAMMA airborne field campaign. *Atmos. Chem. Phys. Disc.* **11**, 723–740.
- Christopher, S. A., Gupta, P., Haywood, J. and Greed, G. 2008. Aerosol optical thicknesses over North Africa: 1. Development of a product for model validation using Ozone Monitoring Instrument, Multiangle

- Imaging Spectroradiometer, and Aerosol Robotic Network. *J. Geophys. Res.* **113**, D00C04, doi:10.1029/2007JD009446.
- Claquin, T., Roelandt, C., Kohfeld, K., Harrison, S., Tegen, I. and co-authors. 2003. Radiative forcing of climate by ice-age atmospheric dust. *Clim. Dyn.* **20**, doi: 10.1007/s00382-002-0269-1.
- Cuesta, J., Edouart, D., Mimouni, M., Flamant, P. H., Loth, C. and co-authors. 2008. Multiplatform observations of the seasonal evolution of the Saharan atmospheric boundary layer in Tamanrasset, Algeria, in the framework of the African Monsoon Multidisciplinary Analysis field campaign conducted in 2006. *J. Geophys. Res.* **113**, D00C07, doi:10.1029/2007JD009417.
- Cziczo, D. J., Froyd, K. D., Gallavardin, S. J., Moehler, O., Benz, S. and co-authors. 2009. Deactivation of ice nuclei due to atmospherically relevant surface coating. *Environ. Res. Lett.* **4**, 1–9.
- DeMott, P. J., Sassen, K., Poellet, M. R., Baumgardner, D., Rogers, D. C. and co-authors. 2003. African dust aerosols as atmospheric ice nuclei. *Geophys. Res. Lett.* **30**, 1732, doi:10.1029/2003GL017410.
- Dinter, T., von Hoyningen-Huene, W., Burrows, J. P., Kokhanovsky, A., Bierwirth, E. and co-authors. 2009. Retrieval of aerosol optical thickness for desert conditions using MERIS observations during the SAMUM campaign. *Tellus* **61B**, 229–238.
- Dubovik, O., Sinyuk, A., Lapyonok, T., Holben, B. N., Mishchenko, M. and co-authors. 2006. Application of spheroid models to account for aerosol particle nonsphericity in remote sensing of desert dust. *J. Geophys. Res.* **111**, D11208, doi:10.1029/2005JD006619.
- Engelmann, R., Wandinger, U., Ansmann, U., Müller, D., Zeromskis, E. and co-authors. 2008. Lidar observations of the vertical aerosol flux in the planetary boundary layer. *J. Atmos. Oceanic Technol.* **25**, 1296–1306.
- Engelmann, R., Ansmann, A., Horn, S., Seifert, P., Althausen, D. and co-authors. 2011. Doppler lidar studies of heat island effects on vertical mixing of aerosols during SAMUM-2. *Tellus* **63B**, this issue.
- Esselborn, M., Wirth, M., Fix, A., Tesche, M. and Ehret, G. 2008. Airborne high spectral resolution lidar for measuring aerosol extinction and backscatter coefficients. *Appl. Opt.* **47**, 346–358.
- Esselborn, M., Wirth, M., Fix, A., Weinzierl, B., Rasp, K. and co-authors. 2009. Spatial distribution and optical properties of Saharan dust observed by airborne high spectral resolution lidar during SAMUM 2006. *Tellus* **61B**, 131–143.
- Field, P. R., Möhler, O., Connolly, P., Krämer, M., Cotton, R. and co-authors. 2006. Some ice nucleation characteristics of Asian and Saharan desert dust. *Atmos. Chem. Phys.* **6**, 2991–3006.
- Formenti, P., Andreae, M. O., Lange, L., Roberts, G., Cafmeyer, J. and co-authors. 2001. Saharan dust in Brazil and Suriname during the Large-Scale Biosphere–Atmosphere Experiment in Amazonia (LBA)—Cooperative LBA Regional Experiment (CLAIRE) in March 1998. *J. Geophys. Res.* **106**, D14, doi:10.1029/2000JD900556.
- Forster, P., Ramaswamy, V., Artaxo, P., Bernsten, T., Betts, R. and co-authors. 2007. Chapter 2: Changes in atmospheric constituents and in radiative forcing. In: *Climate Change 2007: The Physical Science Basis. Contribution of Working Group I to the Fourth Assessment Report of the International Panel on Climate Change*, (eds. S. Solomon, D. Qin, M. Manning, Z. Chen, M. Marquis, K. B. Averyth, M. Tigner and H. L. Miller), Cambridge University Press, Cambridge, United Kingdom and New York, NY, USA., 996pp.
- Freudenthaler, V., Esselborn, M., Wiegner, M., Heese, B., Tesche, M. and co-authors. 2009. Depolarization ratio profiling at several wavelengths in pure Saharan dust during SAMUM 2006. *Tellus* **61B**, 165–179.
- Ganor, E. and Mamane, Y. 1982. Transport of Saharan dust across the eastern Mediterranean. *Atmos. Environ.* **16**, 581–587.
- Ganor, E., Osetinsky, I., Stupp, A. and Alpert, P. 2010. Increasing trend of African dust, over 49 years, in the eastern Mediterranean. *J. Geophys. Res.* **115**, D07201, doi:10.1029/2009JD012500.
- Gasteiger, J., Wiegner, M., Groß, S., Freudenthaler, V., Toledano, C. V. and co-authors. 2011. Modeling lidar-relevant optical properties of complex mineral dust aerosols. *Tellus* **63B**, this issue.
- Gobbi, G. P., Barnaba, F., Giorgi, R. and Santacasa, A. 2000. Altitude-resolved properties of a Saharan dust event over the Mediterranean. *Atmos. Environ.* **34**, 5119–5127.
- Goudie, A. S. and Middleton, N. J. 2001. Saharan dust storms: nature and consequences. *Earth–Sci. Rev.* **56**, 179–204.
- Grassl, H. 1970. Determination of cloud drop size distributions from spectral transmission measurements. *Contr. Atmos. Phys.* **43**, 255–284.
- Groß, S., Tesche, M., Freudenthaler, V., Toledano, C., Wiegner, M. and co-authors. 2011a. Characterization of Saharan dust, marine aerosols and a mixture of biomass burning aerosols and dust by means of multi-wavelength depolarization and Raman lidar measurements during SAMUM-2. *Tellus* **63B**, this issue.
- Groß, S., Gasteiger, J., Freudenthaler, V., Wiegner, M., Geiß, A. and co-authors. 2011b. Characterization of the planetary boundary layer during SAMUM-2 by means of lidar measurements. *Tellus* **63B**, this issue.
- Hamonou, E. P., Chazette, P., Balis, D., Dulac, F., Schneider, X. and co-authors. 1999. Characterization of the vertical structure of Saharan dust export to the Mediterranean basin. *J. Geophys. Res.* **104**, D18, doi:10.1029/1999JD900257.
- Haywood, J. M., Allan, R. P., Culverwell, I., Slingo, T., Milton, S. and co-authors. 2005. Can desert dust explain the outgoing longwave radiation anomaly over the Sahara during July 2003? *J. Geophys. Res.* **110**, D05105, doi:10.1029/2004JD005232.
- Haywood, J. M., Pelon, J., Formenti, P., Bharmal, N., Brooks, M. and co-authors. 2008. Overview of the Dust and Biomass-burning Experiment and African Monsoon Multidisciplinary Analysis Special Observing Period-0. *J. Geophys. Res.* **113**, D00C17, doi:10.1029/2008JD010077.
- Heese, B. and Wiegner, M. 2008. Vertical aerosol profiles from Raman polarization lidar observations during the dry season AMMA field campaign. *J. Geophys. Res.* **113**, D00C11, doi:10.1029/2007JD009487.
- Heese, B., Althausen, D., Dinter, T., Esselborn, M., Müller, T. and co-authors. 2009. Vertically resolved dust optical properties during SAMUM: Tinfou compared to Ouarzazate. *Tellus* **61B**, 195–205.
- Heinold, B., Helmert, J., Hellmuth, O., Wolke, R., Ansmann, A. and co-authors. 2007. Regional modeling of Saharan dust events using LM-MUSCAT: model description and case studies. *J. Geophys. Res.* **112**, D11204, doi:10.1029/2006JD007443.
- Heinold, B., Tegen, I., Schepanski, K. and Hellmuth, O. 2008. Dust radiative feedback on Saharan boundary layer dynamics and dust mobilization. *Geophys. Res. Lett.* **35**, L20817, doi:10.1029/2008GL035319.
- Heinold, B., Tegen, I., Esselborn, M., Kandler, K., Knippertz, P. and co-authors. 2009. Regional Saharan dust modelling during the SAMUM 2006 campaign. *Tellus* **61B**, 307–324.

- Heinold, B., Tegen, I., Schepanski, K., Tesche, M., Esselborn, M. and co-authors. 2011a. Regional modelling of Saharan dust and biomass burning smoke—part 1: model description and validation. *Tellus* **63B**, this issue.
- Heinold, B., Tegen, I., Bauer, S. and Wendisch, M. 2011b. Regional modelling of Saharan dust and biomass burning smoke—part 2: direct radiative forcing and atmospheric dynamic response. *Tellus* **63B**, this issue.
- Heintzenberg, J. 2009. The SAMUM-1 experiment over Southern Morocco: overview and introduction. *Tellus* **61B**, 2–11.
- Helmert, J., Heinold, B., Tegen, I., Hellmuth, O. and Wendisch, M. 2007. On the direct and semi-direct effect of Saharan dust over Europe: a case study. *J. Geophys. Res.* **112**, D13208, doi:10.1029/2006JD007444.
- Holben, B. N., Eck, T. F., Slutsker, I., Tanré, D., Buis, J. P. and co-authors. 1998. AERONET: a federated instrument network and data archive for aerosol characterization. *Remote Sens. Environ.* **66**, 1–16.
- Holben, B. N., Tanré, D., Smirnov, A., Eck, T. F., Slutsker, I. and co-authors. 2001. An emerging ground-based aerosol climatology: aerosol optical depth from AERONET. *J. Geophys. Res.* **106**, D11, doi:10.1029/2000JD900609.
- Huebert, B. J., Bates, T., Russell, P. B., Shi, G., Kim, Y. J. and co-authors. 2003. An overview of ACE-Asia: strategies for quantifying the relationships between Asian aerosols and their climatic impacts. *J. Geophys. Res.* **108**, 8633, doi:10.1029/2003JD003550.
- Jaenicke, R. and Junge, C. 1967. Studien zur oberen Grenzgröße des natürlichen Aerosols. *Contr. Atmos. Phys.* **40**, 129–143.
- Johnson, B. T., Heese, B., McFarlane, S. A., Chazette, P., Jones, A. and co-authors. 2008a. Vertical distribution and radiative effects of mineral dust and biomass burning aerosol over West Africa during DABEX. *J. Geophys. Res.* **113**, D00C12, doi:10.1029/2008JD009848.
- Johnson, B. T., Osborne, S. R., Haywood, J. M. and Harrison, M. A. J. 2008b. Aircraft measurements of biomass burning aerosol over West Africa during DABEX. *J. Geophys. Res.* **113**, D00C06, doi:10.1029/2008JD009451.
- Johnson, B. T., Brooks, M. E., Walters, D., Woodward, S., Christopher, S. and co-authors. 2011. Assessment of the Met Office dust forecast model using observations from the GEBRILS campaign. *Q. J. R. Meteorol. Soc.* **137**, doi:10.1002/qj.736.
- Kaaden, N., Massling, A., Schladitz, A., Müller, T., Kandler, K. and co-authors. 2009. State of mixing, shape factor, number size distribution, and hygroscopic growth of the Saharan anthropogenic and mineral dust aerosol at Tinfou, Morocco. *Tellus* **61B**, 51–63.
- Kahn, R. A., Petzold, A., Wendisch, M., Bierwirth, E., Dinter, T. and co-authors. 2009. Desert dust aerosol mass mapping in the western Sahara, using particle properties derived from space-based multi-angle imaging. *Tellus* **61B**, 239–251.
- Kandler, K., Benker, N., Bundke, U., Cuevas, E., Ebert, M. and co-authors. 2007. Chemical composition and complex refractive index of Saharan Mineral Dust at Izana, Tenerife (Spain) derived by electron microscopy. *Atmos. Environ.* **41**, 8058–8074.
- Kandler, K., Schütz, L., Deutscher, C., Ebert, M., Hofmann, H. and co-authors. 2009. Size distributions, mass concentration, chemical and mineralogical composition and derived optical parameters of the boundary layer aerosol at Tinfou, Morocco, during SAMUM 2006. *Tellus* **61B**, 32–50.
- Kandler, K., Schütz, L., Jäckel, S., Lieke, K., Emmel, C. and co-authors. 2011a. Ground-based off-line aerosol measurements at Praia, Cape Verde, during the Saharan Mineral Dust Experiment: microphysical properties and mineralogy. *Tellus* **63B**, this issue.
- Kandler, K., Lieke, K., Benker, N., Emmel, C., Küpper, M. and co-authors. 2011b. Electron microscopy of particles collected at Praia, Cape Verde, during the Saharan Mineral Dust Experiment: Particle chemistry, shape, mixing state and complex refractive index. *Tellus* **63B**, this issue.
- Kaufman, Y. J., Koren, I., Remer, L. A., Tanré, D., Ginoux, P. and co-authors. 2005. Dust transport and deposition observed from the Terra-Moderate Resolution Imaging Spectroradiometer (MODIS) spacecraft over the Atlantic Ocean. *J. Geophys. Res.* **110**, D10S12, doi:10.1029/2003JD004436.
- Knippertz, P., Deutscher, C., Kandler, K., Müller, T., Schulz, O. and co-authors. 2007. Dust mobilization due to density currents in the Atlas region: observations from the Saharan Mineral Dust Experiment 2006 field campaign. *J. Geophys. Res.* **112**, D21109, doi:10.1029/2007JD008774.
- Knippertz, P., Trentmann, J. and Seifert, A. 2009. High-resolution simulations of convective cold pools over the northwestern Sahara. *J. Geophys. Res.* **114**, D08110, doi:10.1020/2008JD011271.
- Knippertz, P., Tesche, M., Heinold, B., Kandler, K., Toledano, C. and co-authors. 2011. Dust mobilization and aerosol transport from West Africa to Cape Verde: a meteorological overview of SAMUM-2. *Tellus* **63B**, this issue.
- Köhler, C. H., Trautmann, T., Lindermeier, E., Vreeling, W., Lieke, K. and co-authors. 2011. Thermal IR radiative properties of mixed mineral dust and biomass aerosol during SAMUM-2. *Tellus* **63B**, this issue.
- Kohfeld, K. E. and Harrison, S. P. 2001. DIRTMAP: the geological record of dust. *Earth-Sci. Rev.* **54**, 81–114.
- Laurent, B., Tegen, I., Heinold, B., Schepanski, K., Weinzierl, B. and co-authors. 2010. A model study of Saharan dust emissions and distributions during SAMUM-1 campaign. *J. Geophys. Res.* **115**, D21210, doi:10.1029/2009JD012995.
- Levin, Z., Ganor, E. and Gladstein, V. 1996. The effects of desert particles coated with sulfate on rain formation in the eastern Mediterranean. *J. Appl. Meteorol.* **35**, 1511–1523.
- Li, J., Pósfai, M., Hobbs, P. V. and Buseck, P. R. 2003. Individual aerosol particles from biomass burning in southern Africa: 2, compositions and aging of inorganic particles. *J. Geophys. Res.* **108**, 8484, doi:10.1029/2002JD002310.
- Liao, H. and Seinfeld, J. H. 1998. Radiative forcing by mineral dust aerosols: sensitivity to key variables. *J. Geophys. Res.* **103**, D24, doi:10.1029/2006JD0074431998JD200036.
- Lieke, K., Kandler, K., Scheuvs, D., Emmel, C., von Glahn, C. and co-authors. 2011. Particle chemical properties in the vertical column based on aircraft observations in the vicinity of Cape Verde. *Tellus* **63B**, this issue.
- Linke, C., Möhler, O., Veres, A., Mohácsi, Á., Bozóki, Z. and co-authors. 2006. Optical properties and mineralogical composition of different Saharan mineral dust samples: a laboratory study. *Atmos. Chem. Phys.* **6**, 3315–3323.
- Liu, D., Wang, Z., Liu, Z., Winker, D. and Trepte, C., 2008a. A height resolved global view of dust aerosols from the first year CALIPSO lidar measurements. *J. Geophys. Res.* **113**, D16214, doi:10.1029/2007JD009776.

- Liu, Z., Omar, A., Vaughan, M., Hair, J., Kittaka, C. and co-authors. 2008b. CALIPSO lidar observations of the optical properties of Saharan dust: a case study of long-range transport. *J. Geophys. Res.* **113**, D07207, doi:10.1029/2007JD008878.
- Mahowald, N. M. and Luo, C. 2003. A less dusty future? *Geophys. Res. Lett.* **30**, 1903, doi:10.1029/2003GL017880.
- Maring, H., Savoie, D. L., Izaguirre, M. A., Custals, L. and Reid, J. S. 2003. Mineral dust aerosol size distribution change during atmospheric transport. *J. Geophys. Res.* **108**, 8592, doi:10.1029/2002JD002536.
- McConnell, C. L., Highwood, E. J., Coe, H., Formenti, P., Anderson, B. and co-authors. 2008. Seasonal variations of the physical and optical characteristics of Saharan dust: results from the Dust Outflow and Deposition to the Ocean (DODO) experiment. *J. Geophys. Res.* **113**, D14S05, doi:10.1029/2007JD009606.
- Milton, S. F., Greed, G., Brooks, M. E., Haywood, J., Johnson, B. and co-authors. 2008. Modeled and observed atmospheric radiation balance during the West African dry season: role of mineral dust, biomass burning aerosol, and surface albedo. *J. Geophys. Res.* **113**, D00C02, doi:10.1029/2007JD009741.
- Möhler, O., Benz, S., Saathoff, H., Schnaiter, M., Wagner, R. and co-authors. 2008. The effect of organic coating on the heterogeneous ice nucleation efficiency of mineral dust aerosols. *Environ. Res. Lett.* **3**, 025007, 1–8.
- Moulin, C., Lambert, C. E., Dayan, U., Masson, V., Ramonet, M. and co-authors. 1998. Satellite climatology of African dust transport in the Mediterranean atmosphere. *J. Geophys. Res.* **103**, D11, doi:10.1029/98JD00171.
- Müller, D., Heinold, B., Tesche, M., Tegen, I., Althausen, D. and co-authors. 2009a. EARLINET observations of the 14–22 May long-range dust transport event during SAMUM 2006: validation of results from dust transport modelling. *Tellus* **61B**, 325–339.
- Müller, T., Schladitz, A., Massling, A., Kaaden, N., Kandler, K. and co-authors. 2009b. Spectral absorption coefficients and imaginary parts of refractive indices of Saharan dust during SAMUM-1. *Tellus* **61B**, 78–95.
- Müller, D., Weinzierl, B., Petzold, A., Kandler, K., Ansmann, A. and co-authors. 2010a. Mineral dust observed with AERONET Sun photometer, Raman lidar, and in situ instruments during SAMUM 2006: shape-independent particle properties. *J. Geophys. Res.* **115**, D07202, doi:10.1029/2009JD012520.
- Müller, D., Ansmann, A., Freudenthaler, V., Kandler, K., Toledano, C. and co-authors. 2010b. Mineral dust observed with AERONET Sun photometer, Raman lidar, and in-situ instruments during SAMUM 2006: shape-dependent particle properties. *J. Geophys. Res.* **115**, D11207, doi:10.1029/2009JD012523.
- Müller, T., Schladitz, A., Kandler, K., and Wiedensohler, A. 2011. Spectral particle absorption coefficients, single scattering albedos, and imaginary parts of refractive indices from ground-based in-situ measurements at Cape Verde Island during SAMUM-2. *Tellus* **63B**, this issue.
- Myhre, G. and Stordal, F. 2001. Global sensitivity experiments of the radiative forcing due to mineral aerosols. *J. Geophys. Res.* **106**, D16, doi:10.1029/2000JD900536.
- Myhre, G., Hoyle, C. R., Berglen, T. F., Johnson, B. T. and Haywood, J. M. 2008. Modeling of the solar radiative impact of biomass burning aerosols during the Dust and Biomass-burning Experiment (DABEX). *J. Geophys. Res.* **113**, D00C16, doi:10.1029/2008JD009857.
- Osborne, S. R., Johnson, B. T., Haywood, J. M., Baran, A. J., Harrison, M. A. J. and co-authors. 2008. Physical and optical properties of mineral dust aerosol during the Dust and Biomass-burning Experiment. *J. Geophys. Res.* **113**, D00C03, doi:10.1029/2008JD009551.
- Otto, S., Bierwirth, E., Weinzierl, B., Kandler, K., Esselborn, M. and co-authors. 2009. Solar radiative effects of a Saharan dust plume observed during SAMUM assuming spheroidal model particles. *Tellus* **61B**, 270–298.
- Otto, S., Trautmann, T. and Wendisch, M. 2011. On realistic size equivalence and shape of spheroidal Saharan mineral dust particles applied in solar and thermal radiative transfer calculations. *Atmos. Chem. Phys. Disc.* **11**, 4469–4490.
- Papayannis, A., Amiridis, V., Mona, L., Tsaknakis, G., Balis, D. and co-authors. 2008. Systematic lidar observations of Saharan dust over Europe in the frame of EARLINET (2000–2002). *J. Geophys. Res.* **113**, D10204, doi:10.1029/2007JD009028.
- Pelon, J., Mallet, M., Mariscal, A., Goloub, G., Tanré, D. and co-authors. 2008. Microlidar observations of biomass burning aerosol over Djougou (Benin) during African Monsoon Multidisciplinary Analysis Special Observation Period 0: Dust and Biomass-Burning Experiment. *J. Geophys. Res.* **113**, D00C18, doi:10.1029/2008JD009976.
- Pérez, C., Nickovic, S., Pejanovic, G., Baldasano, J. M. and Özsoy, E. 2006. Interactive dust–radiation modeling: a step to improve weather forecasts. *J. Geophys. Res.* **111**, D16206, doi:10.1029/2005JD006717.
- Persson, C., Rodhe, H. and De Geer, L.-E. 1987. The Chernobyl accident: a meteorological analysis of how radionuclides reached and were deposited in Sweden. *AMBIO*. **16**, 20–31.
- Petzold, A., Weinzierl, B., Huntrieser, H., Stohl, A., Real, E. and co-authors. 2007. Perturbation of the European free troposphere aerosol by North American forest fire plumes during the ICARTT-ITOP experiment in summer 2004. *Atmos. Chem. Phys.* **7**, 5105–5127.
- Petzold, A., Rasp, K., Weinzierl, B., Esselborn, M., Hamburger, T. and co-authors. 2009. Saharan dust absorption and refractive index from aircraft-based observations during SAMUM 2006. *Tellus* **61B**, 118–130.
- Petzold, A., Veira, A., Mund, S., Esselborn, M., Kiemle, C. and co-authors. 2011. Mixing of mineral dust with urban pollution aerosol over Dakar (Senegal): impact on dust physico-chemical and radiative properties. *Tellus* **63B**, this issue.
- Prospero, J. M. and Carlson, T. N. 1972. Vertical and areal distribution of Saharan dust over the western equatorial North Atlantic Ocean. *J. Geophys. Res.* **77**, 5255–5265.
- Prospero, J. M., Glaccum, R. A. and Nees, R. T. 1981. Atmospheric transport of soil dust from Africa to South America. *Nature* **289**, 570–572.
- Prospero, J. M., Ginoux, P., Torres, O., Nicholson, S. E. and Gill, T. E. 2002. Environmental characterization of global sources of atmospheric soil dust identification with the Nimbus 7 Total Ozone Mapping Spectrometer (TOMS) absorbing aerosol product. *Rev. Geophys.* **40**, 1002, doi:10.1029/2000RG000095.
- Pruppacher, H. R. and Klett, J. D. 1997. *Microphysics of clouds and precipitation*, Kluwer Academic Publishers, Dordrecht/Boston/London, 954pp.
- Quinn, P. K., Anderson, T. L., Bates, T. S., Dlugi, R., Heintzenberg, J. and co-authors. 1996. Closure in tropospheric aerosol-climate research:

- a review and future needs for addressing aerosol direct shortwave radiative forcing. *Contrib. Atmos. Phys.* **69**, 547–577.
- Ramanathan, V. M., Crutzen, P. J., Lelieveld, J., Mitra, A. P., Althausen, D. and co-authors. 2001. Indian Ocean Experiment: an integrated analysis of the climate forcing and effects of the great Indo–Asian haze. *J. Geophys. Res.* **106**, D22, doi:10.1029/2001JD900133.
- Raes, F., Bates, T., McGovern, F. and Liederkerke, M. V. 2000. The Second Aerosol Characterization Experiment (ACE-2): general overview and main results. *Tellus* **52B**, 111–125.
- Rea, D. K. 1994. The paleoclimatic record provided by eolian deposition in the deep sea: the geologic history of wind. *Rev. Geophys.* **32**, doi:10.1029/93RG03257.
- Redelsperger, J.-L., Thorncroft, C. D., Diedhiou, A., Lebel, T., Parker, D. J. and co-authors. 2006. African Monsoon Multidisciplinary Analysis: an international research project and field campaign. *Bull. Am. Meteorol. Soc.* **87**, 1739–1746.
- Reid, J. S. and Maring, H. B. 2003. Foreword to special section on the Puerto Rico Dust Experiment (PRIDE). *J. Geophys. Res.* **108**, 8585, doi:10.1029/2003JD003510.
- Reid, J. S., Kinney, J. E., Westphal, D. L., Holben, B. N., Welton, E. J. and co-authors. 2003. Analysis of measurements of Saharan dust by airborne and ground-based remote sensing methods during the Puerto Rico Dust Experiment (PRIDE). *J. Geophys. Res.* **108**, 8586, doi:10.1029/2002JD002493.
- Reid, J. S., Piketh, S. J., Walker, A. L., Burger, R. P., Ross, K. E. and co-authors. 2008. An overview of UAE flight operations: observations of summertime atmospheric thermodynamics and aerosol profiles of the southern Arabian Gulf. *J. Geophys. Res.* **113**, D14213, doi:10.1029/2007JD009435.
- Reinfried, F., Tegen, I., Heinold, B., Hellmuth, O., Schepanski, K. and co-authors. 2009. Simulations of convectively-driven density currents in the Atlas region using a regional model: impacts on dust emission and sensitivity to horizontal resolution and convection schemes. *J. Geophys. Res.* **114**, D08127, doi:10.1029/2008JD010844.
- Russel, P. B. and Heintzenberg, J. 2000. An overview of the ACE–2 clear sky column closure experiment (CLEARCOLUMN). *Tellus* **52B**, 463–483.
- Russell, P. B., Hobbs, P. V. and Stowe, L. L. 1999. Aerosol properties and radiative effects in the United States east coast haze plume: an overview of the Tropospheric Aerosol Radiative Forcing Observational Experiment (TARFOX). *J. Geophys. Res.* **104**, D2, doi:10.1029/1999JD900985.
- Schepanski, K., Tegen, I., Heinold, B., Laurent, B. and Macke, A. 2007. A new Saharan dust source activation frequency map derived from MSG-SEVIRI IR-channels. *Geophys. Res. Lett.* **34**, L18803, doi:10.1029/2007GL030168.
- Schepanski, K., Tegen, I., Todd, M. C., Heinold, B., Bönisch, G. and co-authors. 2009. Meteorological processes forcing Saharan dust emission inferred from MSG-SEVIRI observations of subdaily dust source activation and numerical models. *J. Geophys. Res.* **114**, D10201, doi:10.1029/2008JD010325.
- Scheuvs, D., Kandler, K., Küpper, M., Lieke, K., Zorn, S. R. and co-authors. 2011. Individual-particle analysis of airborne dust samples collected over Morocco in 2006 during SAMUM 1. *Tellus* **63B**, this issue.
- Schlادitz, A., Müller, T., Massling, A., Kaaden, N., Kandler, K. and co-authors. 2009. In situ measurements of optical properties at Tinfou (Morocco) during the Saharan Mineral Dust Experiment SAMUM 2006. *Tellus* **61B**, 64–78.
- Schlادitz, A., Müller, T., Nowak, A., Kandler, K., Lieke, K. and co-authors. 2011a. In-situ aerosol characterization at Cape Verde, part 1: particle number size distributions, hygroscopic growth, and state of mixing of the marine and Saharan dust aerosol. *Tellus* **63B**, this issue.
- Schlادitz, A., Müller, T., Nordmann, S., Tesche, M., Groß, S. and co-authors. 2011b. In situ aerosol characterization at Cape Verde, part 2: parameterization of relative humidity- and wavelength-dependent aerosol optical properties. *Tellus* **63B**, this issue.
- Seifert, P., Ansmann, A., Mattis, I., Wandinger, U., Tesche, M. and co-authors. 2010. Saharan dust and heterogeneous ice formation: eleven years of cloud observations at a central-European EARLINET site. *J. Geophys. Res.* **115**, D20201, doi:10.1029/2009JD013222.
- Sokolik, I. and Toon, O. 1999. Incorporation of mineralogical composition into models of the radiative properties of mineral aerosol from UV to IR wavelengths. *J. Geophys. Res.* **106**, D8, doi:10.1029/1998JD200048.
- Sokolik, I., Winker, D. M., Bergametti, G., Kaufman, Y. J., Gomes, L. and co-authors. 2001. Introduction to special section: outstanding problems in quantifying the radiative impacts of mineral dust. *J. Geophys. Res.* **106**, D16, doi:10.1029/2000JD900498.
- Swap, R., Garsting, M., Greco, S., Talbot, R. and Kållberg, P. 1992. Saharan dust in the Amazon basin. *Tellus* **44B**, 133–149.
- Swap, R., Ulanski, S., Cobbett, M. and Garstang, M. 1996. Temporal and spatial characteristics of Saharan dust outbreaks. *J. Geophys. Res.* **101**, D2, doi:10.1029/95JD03236.
- Talbot, R. W., Harriss, R. C., Browell, E. V., Gregory, G. L., Sebacher, D. I. and co-authors. 1986. Distribution and geochemistry of aerosols in the tropical North Atlantic troposphere: relation to Saharan dust. *J. Geophys. Res.* **91**, D4, doi:10.1029/JD091iD04p05173.
- Tanré, D., Haywood, J., Pelon, J., Léon, J.-F., Chatenet, B. and co-authors. 2003. Measurements and modeling of the Saharan dust radiative impact: overview of the Saharan Dust Experiment (SHADE). *J. Geophys. Res.* **108**, 8574, doi:10.1029/2002JD003273.
- Tegen, I., Laci, A. A. and Fung, I. 1996. The influence on climate forcing of mineral aerosols from disturbed soils. *Nature* **380**, 419–422.
- Tegen, I., Werner, M., Harrison, S. P. and Kohfeld, K. E. 2004. Relative importance of climate and land use in determining present and future global soil dust emission. *Geophys. Res. Lett.* **31**, L05105, doi:10.1029/2003GL019216.
- Tegen, I. and Schepanski, K. 2009. The global distribution of mineral dust. *IOP Conf. Series: Earth Environ. Sci.* **7**, doi:10.1088/1755-1307/7/1/012001.
- Tegen, I., Bierwirth, E., Heinold, B., Helmert, J. and Wendisch, M. 2010. The effect of measured surface albedo on modeled Saharan dust solar radiative forcing. *J. Geophys. Res.* **116**, D24312, doi:10.1029/2009JD013764.
- Tesche, M., Ansmann, A., Müller, D., Althausen, D., Mattis, I. and co-authors. 2009a. Vertical profiling of Saharan dust with Raman lidars and airborne HSRL in southern Morocco during SAMUM. *Tellus* **61B**, 144–164.
- Tesche, M., Ansmann, A., Müller, D., Althausen, D., Engelmann, R. and co-authors. 2009b. Separation of dust and smoke profiles over Cape Verde by using multiwavelength Raman and polarization lidars during SAMUM 2008. *J. Geophys. Res.* **114**, D13202, doi:10.1029/2009JD011862.

- Tesche, M., Groß, S., Ansmann, A., Müller, D., Althausen, D. and co-authors. 2011a. Profiling of Saharan dust and biomass-burning smoke with multiwavelength polarization Raman lidar at Cape Verde. *Tellus* **63B**, this issue.
- Tesche, M., Müller, D., Groß, S., Ansmann, A., Althausen, D. and co-authors. 2011b. Optical and microphysical properties of smoke over Cape Verde inferred from multiwavelength lidar measurements. *Tellus* **63B**, this issue.
- Toledano, C., Wiegner, M., Garhammer, M., Seefeldner, M., Gasteiger, J. and co-authors. 2009. Spectral aerosol optical depth characterization of desert dust during SAMUM 2006. *Tellus* **61B**, 216–228.
- Toledano, C., Wiegner, M., Groß, S., Freudenthaler, V., Gasteiger, J. and co-authors. 2011. Optical properties of aerosol mixtures derived from sun-sky radiometry during SAMUM-2. *Tellus* **63B**, this issue.
- Torge, A., Macke, A., Heinold, B. and Wauer, J. 2011. Solar radiative transfer simulations in Saharan dust plumes: particle shapes and 3D effect. *Tellus* **63B**, this issue.
- von Hoyningen-Huene, W., Dinter, T., Kokhanovsky, A., Burrows, J. P., Wendisch, M. and co-authors. 2009. Measurements of desert dust optical characteristics at Porte au Sahara during SAMUM. *Tellus* **61B**, 206–215.
- Wagner, F., Bortoli, D., Pereira, S., Costa, M. J., Silva, A. M. and co-authors. 2009. Properties of dust aerosol particles transported to Portugal from the Sahara desert. *Tellus* **61B**, 297–306.
- Wandinger, U., Tesche, M., Seifert, P., Ansmann, A., Müller, D. and co-authors. 2010. Size matters: influence of multiple scattering on CALIPSO light-extinction profiling in desert dust. *Geophys. Res. Lett.* **37**, L10801, doi:10.1029/2010GL042815.
- Weinzierl, B., Petzold, A., Esselborn, M., Wirth, M., Rasp, K. and co-authors. 2009. Airborne measurements of dust layer properties, particle size distribution and mixing state of Saharan dust during SAMUM 2006. *Tellus* **61B**, 96–117.
- Weinzierl, B., Sauer, D., Esselborn, M., Petzold, A., Veira, A. and co-authors. 2011. Microphysical and optical properties of dust and tropical biomass burning aerosol layers in the Cape Verde region: an overview of the airborne in situ and lidar measurements during SAMUM-2. *Tellus* **63B**, this issue.
- Wiegner, M., Gasteiger, J., Kandler, K., Weinzierl, B., Rasp, K. and co-authors. 2009. Numerical simulations of optical properties of Saharan dust aerosols with emphasis on lidar applications. *Tellus* **61B**, 180–194.
- Winker, D. M., Vaughan, M. A., Hu, Y., Powell, K. A., Liu, Z. and co-authors. 2009. Overview of the CALIPSO mission and CALIOP data processing algorithms. *J. Atmos. Ocean. Tech.* **26**, 2310–2323.
- Woodward, S., Roberts, D. L. and Betts, R. A. 2005. A simulation of the effect of climate change induced desertification on mineral dust aerosol. *Geophys. Res. Lett.* **32**, L18810, doi:10.1029/2005GL023482.
- Wurzler, S., Reisin, T. G. and Levin, Z. 2000. Modification of mineral dust particles by cloud processing and subsequent effects on drop size distributions. *J. Geophys. Res.* **105**, D4, doi:10.1029/1999JD900980.
- Yoshioka, M., Mahowald, N., Dufresne, J. L. and Luo, C. 2005. Simulation of absorbing aerosol indices for African dust. *J. Geophys. Res.* **110**, D18S17, doi:10.1029/2004JD005276.